NANODERM

Quality of Skin as a Barrier to ultra-fine Particles

QLK4-CT-2002-02678

Final Report

2007

Authors:

Tilman Butz (Coordinator)

Tilo Reinert

Teresa Pinheiro

Philippe Moretto

Jan Pallon

Árpad Zoltán Kiss

Jerzy Stachura

Wojciech Dąbroś

Zbigniew Stachura

Janusz Lekki

Malgorzata Lekka

Janos Hunyadi

Tamás Bíró

Michael Sticherling

Luc Van Vaeck

Pieter Van Royen

Jean-Etienne Surlève-Bazeille

Table of Content

Chapter 1

Introduction

Nanoparticles are widely used nowadays and their use is expected to grow rapidly. Their impact on human health has been of concern right away from their introduction to the market [Lan97, Eng04]. Whereas inhalation as the prominent port of entry into the body is studied extensively, little is known about ingestions and percutaneous incorporation is discussed controversely in the literature.

Previous studies were carried out with static Franz-cell systems where excised skin acts as a sort of membrane between applied substance on the *stratum corneum* on one side and a liquid on the other side which is collected and analyzed [Gam06]. Such devices are standardized and commonly used for permeability studies of molecular species. Although there is agreement that molecules heavier than about 0.5 to 1 kD do not penetrate into vital tissue [Mag04], there are numerous reports on the penetration of nanoparticles through skin whose weight greatly exceeds this threshold. The advantage of Franz-cells is that a quantitative integral analysis is possible. The disadvantage is that no information about penetration pathways is obtainable and a diffusion through a hair follicle, e.g., which presumably is truncated on the dermal side, may serve as a channel. In this case, the "apparent" measured penetration in this *in-vitro* experiment does not allow conclusions on *in-vivo* penetration.

Another standard method is tape-stripping. If normalized to the stripped amount of the *stratum corneum*, quantification is possible [Wei99]. However, no depth information is obtainable due to corrugation, furrows, and hair follicles. Furthermore, high resolution electron microscopy (HRTEM) studies on ultra-thin skin cross-sections were carried out, most but not all of which reported penetration into the topmost layers of the *stratum corneum* only [Tan96, Pfl01, Sch02]. The advantage of HRTEM is that individual particles can be visualized – and also analyzed by energy dispersive X-ray detection . The disadvantage is that several preparation steps are involved which could lead to preparation artefacts and ultra-thin cross-sections with a rather small field of view are required which limit the possibility to observe pathways. Furthermore, they raise the question about the significance of observations which could only be overcome by a large number of analyzed samples. Nevertheless, ultrastructural studies by HRTEM are indispensable. A relatively new and promising application is confocal laser scanning microscopy which, however, requires a fluorescent label with the associated problem of the stability of the label [Lad03, Str06].

The objective of the NANODERM project was to complement HRTEM studies with

another technique, namely ion beam analysis (PIXE: Particle Induced X-Ray Emission; RBS: Rutherford Backscattering Spectrometry; STIM: Scanning Transmission Ion Microscopy), in order to visualize putative pathways of nanoparticles in skin cross-sections. The advantage of these techniques is that very few sample preparation steps are required and thus the risk for preparation artefacts is reduced. A further advantage is that preparation artefacts, should they occur, can be easily identified, contrary to HRTEM. Moreover, larger samples can be analyzed in order to get an overview over large areas; subsequently one can zoom into a region of interest [Gon04, Mav07]. A disadvantage is that individual nanoparticles cannot be visualized and the measurements are time-consuming. A further disadvantage is that the sample integrity can suffer if too high currents are used for PIXE; therefore the samples have to be analyzed by STIM, a technique which uses currents of about 0.1 fA before and after the PIXE measurement to ensure sample integrity.

A third technique was foreseen which has not been used thus far for dermal penetration studies: autoradiography using skin cross-sections and microemulsions. For these studies a suitable positron or electron emitter is required. These methods have extreme sensitivity. In order to learn whether nanoparticles in various formulations may react to give new chemical species at a trace level without and with UV-light, ultrasensitive techniques like static SIMS and laser modulated mass spectrometry (LMMS) were employed.

In the project we have also foreseen *in-vitro* and *in-vivo* studies of tissue and cells in contact with nanoparticles provided there is penetration into vital tissue. The corresponding workpackages were activated because occasionally nanoparticles were found to be in close contact with the *stratum granulosum* and *stratum spinosum* or even in the dermis and we could not exclude in all cases that these were preparation artefacts. In addition we wanted to know whether such contacts of nanoparticles with cells in vital tissue yield deleterious effects which should be avoided under all circumstances. Standard immuno-histochemical methods were employed. Finally, elastic properties of vital skin cells were investigated by atomic force microscopy (AFM).

We concentrated our research on TiO_2 nanoparticles in sunscreens, a product which is widely used worldwide, and left out amorphous silicon dioxide - as planned originally - for the following reasons: first, amorphous silicon dioxide nanoparticles are used in food and no harmful effects have ever been reported; second, such particles are much better soluble as their crystalline counterparts, hence they would loose their particle nature rapidly; third, the minimum detection limit for silicon by PIXE is worse than for titanium and it would not be worth to carry out such studies regarding the fact that in most cases no titanium was detected beyond the *stratum corneum*.

Very recently, a review article on dermal penetration of cosmetic products including nanoparticles of TiO_2 and ZnO appeared which does not yet contain the results of the NANODERM project [Noh07].

Chapter 2

Materials and Methods

2.1 Formulations

A variety of commercially available products and standard dermatological formulations were selected. The commercial products were: Eucerin Micropigment Crème 15 (Beiersdorf) Eucerin Micropigment Lotion 25 (Beiersdorf) Avène 50 (Pierre Fabre) Anthelios XP SPF60 (Roche Posay)

Occasionally, we ashed these products and analyzed the nanoparticles by HRTEM.

The formulations used were : Liposome dispersion (made by Prof. Müller-Goymann, TU Braunschweig) SG1101 (sunscreen made by Prof. Müller-Goymann, TU Braunschweig) Carbomergel Polyacrylategel Hydrophobic basisgel Isopropylmyristategel Microemulsion (all five from the hospital pharmacy of Leipzig University prepared according to the German Pharmaceutical Codex)

2.2 Nanoparticles of TiO_2

For the formulations from the TU Braunschweig 5 wt% TiO_2 from Tioveil AQ-N was used. This material has dimensions of about 20 nm width and about 100 nm length. We cannot decide whether the lanceolate appearance was due to agglomeration or not. For the formulations of the University of Leipzig we used 5 wt% TiO_2 Eusolex© T-2000 from Merck. This material is coated. It consists of nanoparticles about 20 nm in width and about 100 nm in length. We cannot decide whether the lanceolate appearance was due to agglomeration or not. We also took HRTEM images from P25 (Degussa) but did not use this material in formulations. The nanoparticles had a diameter of about 20 nm and were disc-like. For the S-SIMS and LMMS as well as AFM investigations we used Eusolex© T-2000. TiO_2 (rutile, uncoated, about 20 nm diameter, R-HD2, Huntsman) was used to prepare a powder target for cyclotron irradiation in order to obtain ^{48}V ($T_{1/2}$ = 16 d) labelled nanoparticles. We had to use uncoated material in order to avoid parasitic activities. For the AFM measurements AMT-100 from Tayca© Corp. (average crystallite size of ∼6 nm) was used. For the *in-vitro* studies TiO_2 nanoparticles JA-1 from Tayca© company (ca. 9 nm, anatase, uncoated) were employed.

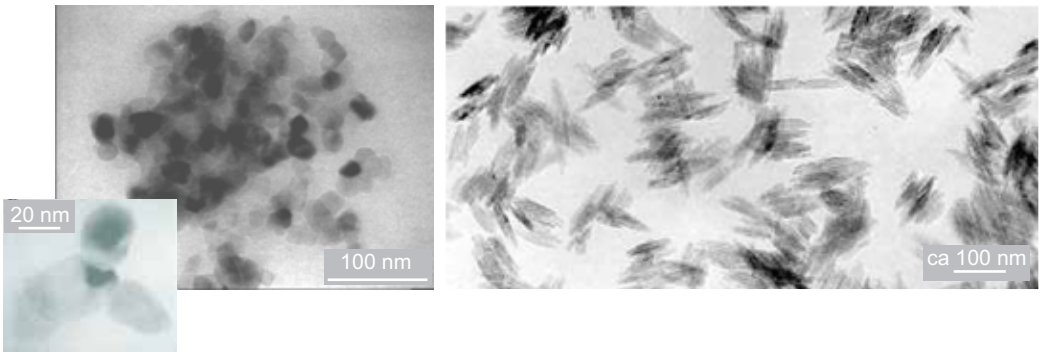

Fig. 2.1: TEM micrographs of TiO_2 nanoparticles from Eucerin© (left) and from Eusolex© T-2000 (right, adapted from MERCK prospectus).

2.3 Skin samples

Skin consists of the *stratum corneum* (flat corneocytes, i.e. dead keratinocytes, with lipids and ceramides between them in a brick-and-mortar fashion. It is usually 10 – 15 µm thick. The first few corneocyte layers are close to desquamation and are held together by desmosomes. This fraction is called *stratum corneum disjunctum* and looks like a cross-section through puff pastry. Below this region, there is a sequence of closely packed corneocyte layers called *stratum corneum compactum*. This layer is followed by a rather thin layer called *stratum lucidum*. Subsequently, there is the *stratum spinosum* which contains vital cells but no blood vessels. These strata together constitute the epidermis. The boundary between epidermis and the underlying dermis with blood vessels and nerves has a papillae-type structure. Hair follicles with sebaceous glands penetrate deeply (0.5 – 1 mm) into the dermis. In addition there are sweat glands. Figure 2.2 shows a simplified scheme of the skin.

We started our investigations with porcine skin, a suitable model for human skin. These samples were obtained during routine surgery courses of the Veterinary Medical Faculty of Leipzig University by partner 1b. Punch biopsies of 5 mm diameter were taken after exposure (see below) from the inner side of the hind legs. A detailed list of all samples (about 400) including exposure and shipment details is given in 2.1 (porcine skin). Subsequent studies were carried out with healthy human skin from volunteers (Male and female, coloured and Caucasian, different ages). About 20 punch biopsies of 3 mm diameter from dorsal and buttock regions were provided by partner 4 (Lisbon). A detailed list of all samples with details is given in 2.2 (human skin). Partner 3 (Debrecen) has ample expertise with human foreskin transplanted to SCID-mice and provided punch biopsy samples for ion microsopy. Partner 7/8 (Bordeaux) carried out a few studies on skin from mouse pads because they had a relatively thick *stratum granulosum*. We obtained from partner 6 (Medical College, Kraków) human skin samples (about 3 cm × 5 cm) from surgery for the experiment with radio-labelled nanoparticles. After completion of the investigations with healthy human skin we started to investigate human skin with an impaired barrier function. Several punch biopsy samples from patients with psoriatic skin were provided by partner 4 (Lisbon). Details are listed in 2.2 (psoriatic skin). Due to reorganisations in the Rydygier state hospital, skin samples from patients with atopic skin were obtained from partner 5

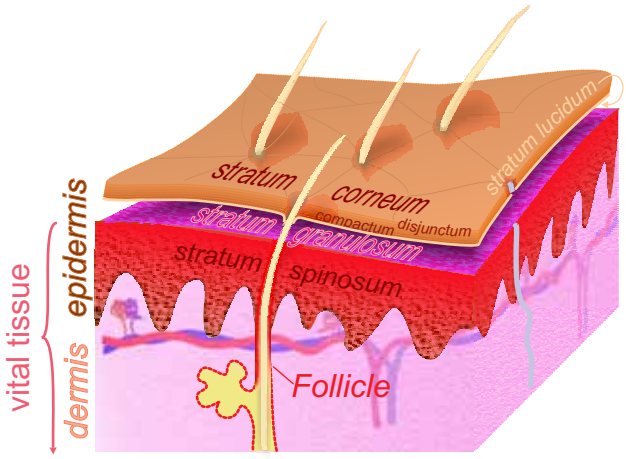

Fig. 2.2: The layered structure of the skin. The epidermis has - in contrast to the dermis - no blood vessels and nerves. However, the *stratum spinosum* and the *stratum granulosum* contain vital cells. The strata (*lucidum* and *compactum*) which do not contain vital cells are schematically lift off for a better clearness.

(IFJ, Kraków) with delay. We plan to carry out a follow-up study on these samples.

Date	Sample	Formulation	Preparation	Time	taken
10.4.2003	1	Eucerin Micro Lot 25		2:00	1
10.4.2003	2	Eucerin Micro Lot 25		2:00	1
10.4.2003	3	Eucerin Micro Lot 25		2:00	1
10.4.2003	4	Eucerin Micro Lot 25		2:00	2
10.4.2003	5	Eucerin Micro Lot 25		2:00	0
10.4.2003	6	Eucerin Micro Lot 25		1:00	1
10.4.2003	7	Eucerin Micro Lot 25		1:00	1
10.4.2003	8	Eucerin Micro Lot 25		1:00	1
10.4.2003	9	Eucerin Micro Lot 25		1:00	1
10.4.2003	10				
10.4.2003	11	native			1
10.4.2003	12	native			1
10.4.2003	13	native			1
10.4.2003	14	native			1
10.4.2003	15				
10.4.2003	16	Eucerin Micro Lot 25		0:30	1
10.4.2003	17	Eucerin Micro Lot 25		0:30	1
10.4.2003	18	Eucerin Micro Lot 25		0:30	1
10.4.2003	19	Eucerin Micro Lot 25		0:30	1
10.4.2003	20				
10.4.2003	21	Eucerin Micro Lot 25		0:15	1
10.4.2003	22	Eucerin Micro Lot 25		0:15	1

10.4.2003	23	Eucerin Micro Lot 25		0:15	1
10.4.2003	24	Eucerin Micro Lot 25		0:15	1
10.4.2003	25				
10.4.2003	26	Eucerin Micro Lot 25		2:00	1
10.4.2003	27	Eucerin Micro Lot 25		2:00	1
10.4.2003	28	Eucerin Micro Lot 25		2:00	1
10.4.2003	29				
10.4.2003	30				
10.4.2003	31	Eucerin Micro Lot 25		0:30	1
10.4.2003	32	Eucerin Micro Lot 25		0:30	1
10.4.2003	33	Eucerin Micro Lot 25		0:30	1
10.4.2003	34				
10.4.2003	35				
10.4.2003	36	Eucerin Micro Lot 25		0:15	1
10.4.2003	37	Eucerin Micro Lot 25		0:15	1
10.4.2003	38	Eucerin Micro Lot 25		0:15	1
10.4.2003	39	Eucerin Micro Lot 25			
10.4.2003	40	Eucerin Micro Lot 25			
10.4.2003	41	native			1
10.4.2003	42	native			1
10.4.2003	43	native			1
10.4.2003	44				
10.4.2003	45				
10.4.2003	46				
10.4.2003	47				
10.4.2003	48				
10.4.2003	49				
10.4.2003	50				
11.4.2003	51	Eucerin Micro Lot 25		0:15	1
11.4.2003	52	Eucerin Micro Lot 25		0:21	
11.4.2003	53	Eucerin Micro Lot 25		0:23	1
11.4.2003	54	Eucerin Micro Lot 25		0:25	1
11.4.2003	55	Eucerin Micro Lot 25		0:28	1
11.4.2003	56	Eucerin Micro Lot 25		0:30	1
11.4.2003	57	Eucerin Micro Lot 25		0:33	1
11.4.2003	58	Eucerin Micro Lot 25		0:38	1
11.4.2003	59	Eucerin Micro Lot 25		0:40	1
11.4.2003	60	Eucerin Micro Lot 25		0:43	1
11.4.2003	61	Eucerin Micro Lot 25		0:45	1
11.4.2003	62	Eucerin Micro Lot 25		0:47	1
11.4.2003	63	Eucerin Micro Lot 25		0:49	1
11.4.2003	64	Eucerin Micro Lot 25		0:53	1
11.4.2003	65	Eucerin Micro Lot 25		1:13	1

11.4.2003	66	Eucerin Micro Lot 25		1:16	1
11.4.2003	67	Eucerin Micro Lot 25		1:16	1
11.4.2003	68	Eucerin Micro Lot 25		1:16	1
11.4.2003	69	Eucerin Micro Lot 25		1:16	1
11.4.2003	70	Eucerin Micro Lot 25		1:16	1
11.4.2003	71	Eucerin Micro Lot 25		1:16	1
11.4.2003	72	Eucerin Micro Lot 25		2:11	1
11.4.2003	73	Eucerin Micro Lot 25		2:11	1
11.4.2003	74	Eucerin Micro Lot 25		2:11	1
11.4.2003	75	Eucerin Micro Lot 25		2:11	1
11.4.2003	76	Eucerin Micro Lot 25		2:11	1
11.4.2003	77	Eucerin Micro Lot 25		2:11	1
11.4.2003	78	Eucerin Micro Lot 25		2:11	1
9.10.2003	79	native	-	-	
9.10.2003	80	Eucerin Micropigment 25	-	0:20	8
9.10.2003	81	Eucerin Micropigment 25	tape stripped	0:27	8
9.10.2003	82	Eucerin Micropigment 25	cleaned with ethanol	0:31	8
9.10.2003	83	Eucerin Micropigment 25	water applied	0:36	8
11.10.2003	84	Carbomergel	-	2:07	8
11.10.2003	85	Carbomergel	-	2:07	4
11.10.2003	86	Carbomergel	tape stripped	2:14	8
11.10.2003	87	Carbomergel	tape stripped	2:14	4
11.10.2003	88	Carbomergel	cleaned with ethanol	2:16	8
11.10.2003	89	Carbomergel	cleaned with ethanol	2:16	4
11.10.2003	90	Carbomergel	water applied	2:18	8
11.10.2003	91	Carbomergel	water applied	2:18	4
11.10.2003	92	native	-	2:19	8
11.10.2003	93	native	-	2:20	4
12.10.2003	94	Isopropylmyristatgel	-	2:30	4
12.10.2003	95	Microemulsiongel	-	1:50	4
12.10.2003	96	Microemulsiongel	-	2:10	4
12.10.2003	97	native	-		8
12.10.2003	98	Microemulsiongel	-	1:50	8
12.10.2003	99	Microemulsiongel	water applied	1:55	8
12.10.2003	100	Microemulsiongel	cleaned with ethanol	2:05	8
12.10.2003	101	Microemulsiongel	tape stripped	2:10	8
12.10.2003	102	native	-	-	8
12.10.2003	103	Isopropylmyristatgel	-	2:30	8
12.10.2003	104	Isopropylmyristatgel	water applied	2:35	8
12.10.2003	105	Isopropylmyristatgel	cleaned with ethanol	2:40	8
12.10.2003	106	Isopropylmyristatgel	tape stripped	2:45	8
14.11.2003	107	native	-	-	4
14.11.2003	108	Hydrophobic basisgel	-	1:43	4

14.11.2003	109	Hydrophobic basisgel	water applied	1:48	4
14.11.2003	110	Hydrophobic basisgel	cleaned with ethanol	1:56	4
14.11.2003	111	Hydrophobic basisgel	tape stripped	2:00	4
14.11.2003	112	native	-	-	4
14.11.2003	113	Polyacrylatgel	-	2:07	4
14.11.2003	114	Polyacrylatgel	water applied	2:17	4
14.11.2003	115	Polyacrylatgel	cleaned with ethanol	2:22	4
14.11.2003	116	Polyacrylatgel	tape stripped	2:27	4
14.11.2003	117	native	-	-	4
14.11.2003	118	Hydrophobic basisgel	-	1:43	4
14.11.2003	119	Hydrophobic basisgel	water applied	1:48	4
14.11.2003	120	Hydrophobic basisgel	cleaned with ethanol	1:56	4
14.11.2003	121	Hydrophobic basisgel	tape stripped	2:00	4
14.11.2003	122	native	-	-	4
14.11.2003	123	Polyacrylatgel	-	2:07	4
14.11.2003	124	Polyacrylatgel	water applied	2:17	4
14.11.2003	125	Polyacrylatgel	cleaned with ethanol	2:22	4
14.11.2003	126	Polyacrylatgel	tape stripped	2:27	4
14.11.2003	127	lost			
14.11.2003	128	Hydrophobic basisgel	-	1:43	8
14.11.2003	129	Hydrophobic basisgel	water applied	1:48	8
14.11.2003	130	Hydrophobic basisgel	cleaned with ethanol	1:56	8
14.11.2003	131	Hydrophobic basisgel	tape stripped	2:00	8
14.11.2003	132	native	-	-	
14.11.2003	133	Polyacrylatgel	-	2:07	8
14.11.2003	134	Polyacrylatgel	water applied	2:17	8
14.11.2003	135	Polyacrylatgel	cleaned with ethanol	2:22	8
14.11.2003	136	Polyacrylatgel	tape stripped	2:27	8
4.2.2004	137	Microemulsion	tape stripped	03:48	
4.2.2004	138	Isopropylmyristatgel	tape stripped	03:45	
4.2.2004	139	Polyacrylatgel	tape stripped	03:41	
4.2.2004	140	Hydrophobic basisgel	tape stripped	03:37	
4.2.2004	141	Control without stripping			
4.2.2004	142	native	tape stripped		
4.2.2004	143	Microemulsion	tape stripped	03:38	
4.2.2004	144	Isopropylmyristatgel	tape stripped	03:35	
4.2.2004	145	Polyacrylatgel	tape stripped	03:31	
4.2.2004	146	Hydrophobic basisgel	tape stripped	03:27	
4.2.2004	147	Control without stripping			
4.2.2004	148	native	tape stripped		

Tab. 2.1: Details for pig skin.

Sample	Formulation	Time	Local	Type	Condition
M20	Avène 50	2 h	sacrum	N	Open test; no stripping
M21	Avène 50	2 h	sacrum	N	Open test; no stripping
M22	Hydrophobic basisgel	2 h	sacrum	N	open test; no stripping; no occlusion
M23	Hydrophobic basisgel	2 h	sacrum	N	open test; stripping; no occlusion
M24	Anthelios SPF 60	2 h	sacrum	N	open test; no stripping; no occlusion
M25	Hydrophobic basisgel	2 h	sacrum	N	open test; no stripping; no occlusion
M26	Hydrophobic basisgel	2 h	sacrum	N	open test; no stripping; no occlusion
M27	Hydrophobic basisgel	2 h	sacrum	N	open test; no stripping; no occlusion
M28	Hydrophobic basisgel	2 h	sacrum	N	open test; no stripping; no occlusion
M29	Anthelios SPF 60	2 h	sacrum	N	open test; no stripping; no occlusion
M30	native	2 h	sacrum	N	open test; no stripping; no occlusion
M31	native	2 h	sacrum	N	open test; no stripping; no occlusion
M32	Anthelios SPF 60	2 h	sacrum	N	open test; no stripping; no occlusion
M33	Anthelios SPF 60	2 h	sacrum	N	open test; stripping; no occlusion
M34	Anthelios SPF 60	2 h	sacrum	N	open test; no stripping; no occlusion
M35	native	2 h	sacrum	N	open test; no stripping; no occlusion
M36	Anthelios SPF 60	2 h	Lesion	Psor	open test; no stripping; no occlusion
M37	Anthelios SPF 60	2 h	Lesion	Psor	open test; no stripping; no occlusion
M38	Anthelios SPF 60	2 h	Lesion	Psor	open test; no stripping; no occlusion
M39	Anthelios SPF 60	2 h	Lesion	Psor	open test; no stripping; no occlusion
M40	native	2 h	Sacrum	N	open test; no stripping; no occlusion
M41	native	2 h	Sacrum	N	open test; no stripping; no occlusion
M42	native	2 h	Sacrum	N	open test; no stripping; no occlusion

Tab. 2.2: Details for human skin.

2.4 Exposure protocols and sample preparation

Approximately 2 mg of formulation were applied topically to an area of about 1 cm^2 of skin. Various pre-treatments were used: no pre-treatment (native), cleaning the skin with ethanol (degreasing), exposure to water (hydration), dehydration, partial tape stripping. As we expected to see differences in uptake as a function of exposure time, we varied the exposure time from about 30 minutes up to a maximum of 48 hours. Occlusive conditions as well as non-occlusive conditions were used. Details are given in the table.

The biopsies for ion microscopy were shock-frozen in isopentane chilled with liquid nitrogen, freeze-dried and shipped to the partners. Subsequently cross-sections between 10 and 15 µm were obtained by cryo-microtomes. The cutting direction was from the side of the dermis towards the *stratum corneum* forming an angle of about 45 in order to avoid contaminations from the cutting knife. Cutting parallel to the *stratum corneum* was not useful because the stratum corneum frequently detached from the epidermis. The biopsies for HRTEM and optical microscopy were chemically fixed in glutaraldehyde/cacodylate buffer and shipped to partners 2 (LFDRC, Bordeaux) and 6 (Medical College, Kraków). Ultra-thin cross-sections of about 50 nm thickness were prepared in the HRTEM-laboratories.

Thin cross-sections of about 10 µm were prepared from the excised skin used for autoradiography, dipped into the nuclear microemulsion and stored in the dark for 14 days. Subsequently they were developed following standard procedures.

2.5 Methods

2.5.1 Electron and ion microscopy

HRTEM and ion beam analysis are standard methods and we refer the reader to textbooks [Ful04, Lla98]. Here, it suffices to state that HRTEM requires ultra-thin samples. Usually stains are used to enhance the contrast for morphological studies and individual nanoparticles like TiO_2 are easily detected. With energy-dispersive X-Ray detection the composition of the nanoparticle can be obtained and thus a discrimination against other particles is possible. In ion beam analysis -PIXE yields elemental maps with lateral resolution around 1 µm but has practically no depth sensitivity, RBS yields information on sample thickness and to some extent also composition, and STIM yields density contrast maps with lateral resolutions down to 100 nm. Figure 2.3 gives an overview of the simplified principles of the methods PIXE, RBS, and STIM.

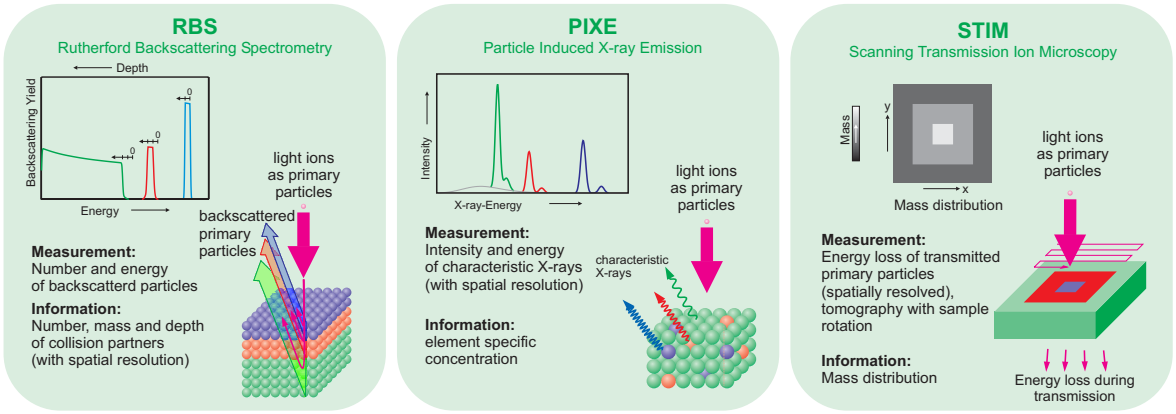

Fig. 2.3: Overview of the simplified principles of the three ion beam analysis methods PIXE, RBS, and STIM. Scanning the focussed proton beam yields the spatial distribution of the signals.

Autoradiography with microemulsions works like film exposure. It does not visualize individual nanoparticles with 20 nm dimensions, but individual positron (or electron) tracks are visible and thus a discrimination between inactive spots and radioactive spots is easy.

For HRTEM no meaningful minimum detection limit can be quoted since a single particle is detectable. The minimum detection limit for Ti which can be detected essentially background-free is 1 – 3 µg/g. This corresponds to about one nanoparticle with dimensions of 20 × 20 × 100 nm^3 in a tissue volume of 10 μm^3 .

2.5.2 Immuno-histochemical techniques

Animals All animal experiments were performed as accepted by our institutional ethical comittee. Experiments on SCID mice were carried out at the Department of Dermatology, University of Debrecen, Medical and Health Science Center (UDMHSC, Debrecen, Hungary) under serum pathogen free conditions. Human foreskin grafts were obtained from circumcision and transplanted onto SCID-mice. The grafts on the mice were treated with TiO_2-emulsion at 2 mg/cm^2 concentration in occlusion for 24 hours

along with untreated control. After exposure time, animals were euthanized. From each graft area, 6 mm diameter skin punch biopsies were taken and were processed for histology and immunohistochemistry.

Histology Cryostat sections (8 μm thick) of skin biopsies and cultured HF were fixed in acetone, air-dried, and processed for histochemistry. Hematoxylin-eosin (HE, Sigma) staining was used for studying HF morphology whereas melanin pigment was visualized by the Masson-Fontana histochemistry.

Immunohistochemistry Immunohistochemistry was performed to define the expression of the proliferation marker bromo-deoxy-uridine (BrdU) in the human skin, certain differentiation markers (keratin-1 and -10, filaggrin), and the cell adhesion molecule P-cadherin both in the human skin and HF samples. In addition, to evaluate apoptotic cells in co-localization with a proliferation marker Ki-67, a Ki-67/TUNEL (Terminal deoxynucleotidyl Transferase Biotin-dUTP Nick End Labeling) double-staining method was employed.

To detect BrdU, a streptavidine-biotin-complex (SABC) three-step immunohistochemical technique was employed. Inhibition of endogenous peroxidase activity was performed using 0.5% H_2O_2 in 100% methanol. Non-specific binding of the antibodies was blocked by 2% bovine serum albumin in phosphate-buffered saline (pH 7.6). Sections were first incubated with an anti-BrdU goat primary antibody, then with a biotin-coupled anti-goat secondary antibody, and, finally, with streptavidine conjugated with horseradish peroxidase. To reveal the peroxidase activity, DAB was employed as a chromogene. Tissue samples were finally slightly counterstained with haematoxylin Gill I and mounted with Aquatex.

For the detection of the differentiation markers and adhesion molecules both in the human skin and hair follicle (HF) samples, an immunofluorescence method was used. Sections were first incubated by the appropriate primary antibodies, then labeled with FITC-labeled species-matched secondary antibodies, and, finally, were counterstained by DAPI. The intensity of fluorescence immunoreactivity in each section was measured at 5 – 5 previously defined reference regions of interest (ROI) at a 0 – 255 unit/pixel intensity range using the Image Pro Plus 4.5.0 software, and the average of the specific immunosignal (mean ± SE) was calculated. A similar approach was employed to define the melanin content of the bulb regions of individual HF, labeled by Masson-Fontana histochemistry.

During the double Ki-67/TUNEL labeling, cryostat sections of the skin or HF were fixed in formalin/ethanol/acetic acid and labeled with a digoxigenin-deoxyUTP in presence of terminal deoxynucleotidyl transferase (TdT), followed by incubation with a mouse anti-Ki-67 antiserum. TUNEL+ cells were visualized by an anti-digoxigenin FITC-conjugated antibody, whereas Ki-67 was detected by a rhodamine-labeled goat anti-mouse antibody. Finally, sections were counterstained by DAPI (1 μg/ml, Boehringer Mannheim). The number of cells positive for Ki-67 and TUNEL immunoreactivity was counted per section and was normalized to the number of total (DAPI+) cells.

Cell culture The human immortalized HaCaT keratinocyte cell line was cultured in 25 cm^2 or 75 cm^2 tissue culture flasks (if not indicated otherwise) in Dulbecco's modified Eagle's medium (DMEM) supplemented with 10% fetal calf serum (FCS), 2 mM/L-glutamine, 50 U/ml penicillin, 50 µg/ml streptomycin, 1.25 µg/ml fungizone at 37C in a 5% CO_2 atmosphere. Human dermal fibroblasts (HDFs) were obtained from de-epidermized dermis using enzymatic digestion and were cultured in the above supplemented DMEM. The human sebaceous gland-derived immortalized sebaceous gland-derived cell line SZ95 was cultured in SeboMed medium supplemented with 10% FCS, 1 mM $CaCl_2$, 5 ng/ml human recombinant epidermal growth factor, 50 U/ml penicillin, 50 µg/ml streptomycin. The primary human melanocytes were cultured in DMEM supplemented with 10% FCS, 2 mmol/l-glutamine, 50 U/ml penicillin, 50 µg/ml streptomycin, 1.25 µg/ml fungizone.

The human hair follicle organ culture Human anagen hair follicles (HF) were isolated from skin obtained from females undergoing face-lift surgery. Isolated HF were maintained in 24-multiwell plates in supplemented Williams E medium supplemented with 2 mM L-glutamine, 10 ng/ml hydrocortisone, 10 µg/ml insulin, and antibiotics. Length measurements were performed on individual HF using a light microscope with an eyepiece measuring graticule.

Determination of cellular proliferation The number of viable cells was determined by measuring the conversion of the tetrazolium salt MTT to formazan. Cells were plated in 96-well multititer plates (5000 cells/well density) in quadruplicates and were treated with different concentrations of TiO_2 for the time indicated. Cells were then incubated with 0.5 mg/ml MTT for 2 hrs, and the concentration of formazan crystal (as the indicator of number of viable cells) was determined colorimetrically according to the manufacturer's protocol. Data are expressed as mean ± SE.

Determination of apoptosis After TiO_2 exposure, cells were collected by trypsinization and were incubated with 1 ml fluorescein FITC-conjugated annexin V for 10 min in darkness. Cells were then measured by a flow cytometer and the percentage of apoptotic cells compared to total cell number was determined.

Determination of necrosis After TiO_2 exposure, cells were collected by the (otherwise) membrane impermeant dye SytoxGreen and the amount of the uptaken labeling agent (reflecting membrane supture) was measured by the Fluorescence Image Microplate Reader (FLIPR). Data are expressed as mean ± SE.

Western blot analysis This measurement was performed to investigate the expression of certain adhesion molecules (desmoglein-1, P-cadherin) and differentiation markers (involucrin). Cells were washed with ice-cold phosphate-buffered saline (PBS), harvested in homogenization buffer and disrupted by sonication on ice. The protein content of samples was measured by a modified BCA protein assay. The samples were subjected to SDS-PAGE (8% gels were loaded with 20 – 30 mg protein per lane) and transferred to nitrocellulose membranes. Membranes were then blocked with 5%

dry milk in PBS and probed with the appropriate primary mouse antibodies against the molecules. A peroxidase-conjugated goat anti-mouse secondary antibody was then applied and the immunoreactive bands were visualized by an ECL Western blotting detection kit on light-sensitive films. To assess equal loading, nitrocellulose membranes were stripped in 200 ml of 50 mM Tris-HCl buffer (pH 7.5) containing 2% SDS and 0.1% β-mercaptoethanol at 65C for 1 h and were re-probed with a mouse anti-cytochrome-c antibody followed by a similar visualization procedure as described above.

Calcium imaging Changes in intracellular calcium concentration ($[Ca^{2+}]_i$) upon TiO_2 exposure were detected in the following way. In brief, a calcium sensitive probe was introduced into the intracellular space by incubating the keratinocytes with 5 mM fura-2 AM for 1 h at 37C. Before each measurement, the cells were kept at room temperature (22 – 24C) in normal Tyrode's solution (in mM; 137 NaCl, 5.4 KCl, 0.5 $MgCl_2$, 1.8 $CaCl_2$, 11.8 HEPES-NaOH, 1 g/l glucose, pH 7.4) for a half an hour to allow homogeneous distribution of the dye. The coverslips, containing the fura-2 loaded cells, were then placed on the stage of an inverted fluorescence microscope. Excitation was altered between 340 and 380 nm using a dual wavelength monochromator (Deltascan, Photon Technology International). The emission was monitored at 510 nm with a photomultiplier at an acquisition rate of 10 Hz per ratio, and the fluorescence ratio (F340/F380) values were determined.

2.5.3 Atomic force microscopy

Atomic force microscopy provides three-dimensional images of the topography of the investigated sample and information about its physical and mechanical properties. In AFM, a sharp small tip, which is attached to a compliant cantilever, is placed almost parallel to the surface and then moved over it, performing a raster scan. The force acting between the tip and the sample causes the cantilever to be deflected, and this deflection may be detected using, for example, a laser beam that is focused at the end of cantilever and then, after reflection from the cantilever, it is detected by a position-sensitive detector (PSD). The position of the beam spot on a PSD surface provides information on cantilever displacement.

Usually, commercially available instruments use a PSD photodiode that has an active area that is divided into four quadrants, which enables the recording of two orthogonal cantilever deflections: a normal one, (perpendicular to the investigated surface, corresponding to surface topography), and a lateral one (torsion, related to frictional forces). The great advantage of the method is that immersion of the sample in (transparent) liquid does not change this principle of operation (see 2.4).

During measurements of the sample stiffness, the AFM tip mounted at the end of the cantilever approaches the surface and indents it. The loading force is controlled by the amount of cantilever deflection and the spring constant. The measurement may be carried out in several different ways.

The most popular method involves force spectroscopy, where so-called force curves are recorded. A force curve gives the relationship between the recorded cantilever deflection and the relative sample position. This dependence can be then converted into

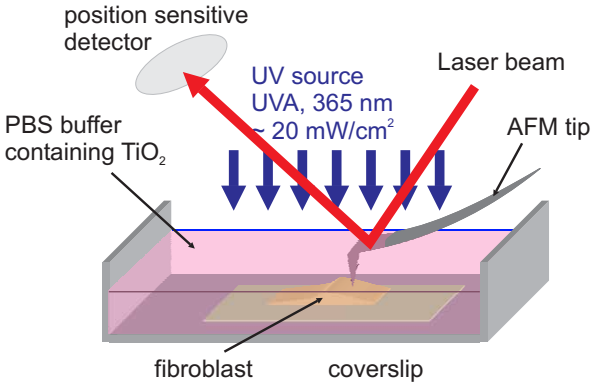

Fig. 2.4: The AFM tip is immersed into the medium to measure the mechanical properties of the cell (e.g. fibroblast). The laser beam, focussed onto the AFM tip, is deflected according to the tip orientation. The position sensitive detector measures the deflection.

a force (load)-indentation curve, which is the basis for the Youngs modulus determination.

The other measuring technique uses AFM in a so-called *nano Swiss cheese* technique that permits the axial and shear moduli to be determined. Although the latter technique was developed primarily for investigations of carbon nanotubes, it can also be successfully applied to biological samples with similar fibrous structures (of course, providing that the experiment is performed in a liquid environment). The force modulation mode can also be applied to determine the mechanical properties of living cells, although this method gives only qualitative results.

Cells are very compliant and complex objects, and so cell indentation generates responses from a variety of cell structural components, including glycocalix, the cell membrane and the interior of cell (the cytoskeleton and organelles immersed in cytosol). The responses from the glycocalix and the cell membrane are the most significant for small indentations (100 nm and less). However, these components are usually not visible in AFM measurements due to their very low compliance and the low accuracy of the contact point determination. The large deformation range is dominated by the responses from the internal cell structures such as cytoskeleton and cellular organelles.

Comparing the dimensions of all interacting objects with the indentation depth suggests that the response of the cellular scaffold is the most important, and therefore the elastic properties measured reflect mainly the properties of the cytoskeleton [Jan95, Lek99]. In order to prove this hypothesis, a lot of effort has been made to investigate the role of cytoskeletal elements in the mechanical properties of the cell. The contribution of the cell cytoskeleton to the mechanical properties determined by AFM has been discussed in several studies, where the importance of both the structural proteins of the cytoskeleton and other proteins associated with the cytoskeleton was demonstrated [Gol98, Bha97].

Since the cell cytoskeleton is composed of three main elements (actin filaments, intermediate filaments and microtubules), their individual roles have been investigated in order to find the main contributor to cell mechanics. The results have shown that the actin filaments are mostly responsible for the mechanical properties observed in AFM measurements, disrupting the microtubules produced no effect on the mechanical

properties of cells as measured by AFM. The role of cytoskeleton-associated proteins in measured cell elasticity has been demonstrated for cells possessing vinculin, a protein that is required for actin stress fiber formation.

The cell elasticity determined via AFM is a very local feature; large discrepancies are seen between the Youngs modulus measured for a population of cells and that for a single cell. It has been reported that cells *in-vitro* have Youngs modulus values in the range of 1 - 100 kPa, which encompasses various types of investigated cells, including vascular smooth muscle cells, fibroblasts, bladder cells, red blood cells, platelets and other epithelial cells.

Since different cell types are being measured, the large variation in Youngs modulus (YM) is easily understood. Despite large errors (defined as the half-width of the YM distribution peak at half maximum, the HWHM), a comparison of the cell elasticity clearly shows a much smaller Youngs modulus (a larger deformability) for cancerous bladder cells than for reference cells [Lek99]. The difference between the YM of these cells was almost one order of magnitude. The significant differences in the YM values found enabled alterations within cell populations arising from the actions of drugs to be traced.

2.5.4 FT LMMS and S-SIMS

This section briefly summarises relevant information on the methodology, instrumental aspects and analytical features of the two methods Fourier Transform Laser Microprobe Mass Spectrometry (FT LMMS) and Static Secondary Ion Mass Spectrometry (S-SIMS). Due to the specific ionisation method (primary ions or laser), the approach is quite different in comparison to that used in conventional mass spectrometry with electron ionisation (EI) or chemical ionisation (CI) in the gas phase. Finally, the combination of the mass spectra and knowledge about ionisation and fragmentation in S-SIMS or FT LMMS allows interaction products in complex system to be traced back and identified.

FT LMMS - Fourier Transform Laser Microprobe Mass Spectrometry

The analysis is based on the use of ns-pulses from a UV laser beam, focused to a spot with diameter of 1 – 5 µm, to irradiate a solid sample at a power density of 10^6 – 10^{10} W/cm^2 and thereby generate ions, which are then mass analysed and detected. The LMMS methodology has been originally introduced in the late 70ies. Early instruments (and commercial versions, e.g. LAMMA from Leybold, LIMA from Kratos) have used a time-of-flight (TOF) mass analyser to optimise transmission and sensitivity, allowing a full mass spectrum to be recorded from a single laser interaction (crater volume is typically 1 µm in diameter, 0.3 – 1 µm deep). Although a TOF instrument has in principle no upper m/z limit (ions up to m/z 10^5 – 10^6 can be transmitted), mass resolution (10% valley) is confined to typically 500 in LMMS. This limits the application to analytes with relatively low MW. Furthermore, insufficient separation power also reduces the possibilities to analyse complex mixtures. Fundamental research at MiTAC has revealed an inherent incompatibility of the time domain for ion formation and that of TOF mass analysis, which prevents to exploit all the analytical sensitivity and

capabilities that focused laser ionisation may offer for micro- and nanoscale analysis of solids.

Therefore, several laboratories have attempted the combination of focused laser irradiation with a high mass resolution FTMS. Most set-ups use ionisation of the sample inside a single or double cell instrument. This option reveals to reduce the potential improvement aimed at in terms of sensitivity, specificity and mass resolution. In 1992 MiTAC has built the first LMMS instrument with external ion source, allowing the cell to be maintained at 10^{-10} Torr for optimal sensitivity and mass resolution.

A laser pulse ($\lambda = 256$ nm, 8 ns) irradiates the sample inside the ion source with spot diameter of 5 mm at a power density of 10^6 –10^{10} W/cm^2. The point of analysis is positioned under microscope observation in the waist of the ionising laser using the x, y, z micromanipulator. The ions are transferred from the source to the FTMS cell by means of static electrical fields for the actual mass analysis.

The cell traps the ions in an electrostatic potential valley of about 2 eV along the axis of a strong magnetic field B (4 – 7 T). The latter forces the ions on circular orbits with a frequency ν_{ion} that is inversely proportional to their m/z. Initially, ions orbit with random phase on trajectories with a diameter $<$ 1 mm. A radio-frequency field with ν_{ion} between the transmitter plates allows the ions to take up energy and widen their trajectory until they orbit close to the receiver plates. The excitation also converts the original random phase of ions with given m/z into phase-coherent orbiting, allowing detectable image currents to be induced in the receiver plates. As a result, a sinusoidal signal with ν_{ion} and amplitude corresponding to the m/z and the number of ions, respectively, is generated. When the trap contains ions of different m/z, Fourier transformation resolves the superposition of individual sinuses into the individual ν-components (m/z) and amplitudes.

The strong B-field causes detectable $\Delta\nu$ for ions with a $\Delta m/z$ in the millimass range. This gives FT-MS an inherent potential for ultra-high mass resolution and mass accuracy on the condition that the signal can be sampled over sufficient periods. Collisions between the ions and neutrals from the residual vacuum, imperfect trapping fields and sometimes space charge effects (too many ions in the cell) cause the phase coherence to vanish with time. Consequently, the signal becomes exponentially damped and its decay rate determines the mass peak width and resolution.

Hence, mass resolution is simply increased by pumping the cell, optimising of the trap voltages (V_{trap}) or reducing of the number of ions. The same actions also improve sensitivity by optimising the phase coherence and spread on the ion orbit radius after excitation. Unlike all other forms of MS, better mass resolution means better sensitivity in FTMS.

The use of the static electric fields to transfer ions from the external ion source to the cell implies that only a limited m/z range can be covered in LMMS. During transfer, ions with different m/z become dispersed in time, i.e. low m/z ions arrive sooner at the cell than the ones with high m/z. Injection into the cell requires the trapping voltage on the front electrode to be reduced. Once inside the cell, ions reflect against the second trapping plate and travel back towards the front plate. If the trapping potential is not restored in time, ions escape again. Simultaneous trapping of ions with different m/z from a single laser pulse requires that the high m/z ions have already entered the cell

before the low m/z ions leave it (after reflection). The so-called T_{gate} parameter (time between laser pulse and closing of the cell) determines which m/z window is covered. Recent redesign of the ion transfer line allowed simultaneous trapping to be extended for ions from m/z 41 to 1000.

Static Secondary Ion Mass Spectrometry S-SIMS

Secondary ion mass spectrometry (SIMS) is based on the mass spectrometric analysis of ions, which are generated by the interaction of a primary ion beam (keV range) with a liquid or solid sample. Unlike neutral beams, primary ion beams can be focused into a sub-micrometer spot for local analysis. There are two operational regimes in SIMS, each of which yields fundamentally different information and analytical features. The so-called dynamic SIMS involves use of a high primary ion current density on the sample. Static SIMS (S-SIMS) operates in principle the same primary ion guns but at low primary ion current. The basic idea of S-SIMS is that each local environment in the sample is hit by only one primary ion.

The true power of S-SIMS for surface analysis emerged when Benninghoven (1970) reduced the primary ion current density on the sample. This allowed detection of structural ions from organic compounds with an information depth limited to the uppermost surface layer. Initially, the benefits of the static regime were primarily explored with quadrupole S-SIMS instruments. An important step in the development was taken by the use of time-of-flight (TOF) analysers. Their high transmission and inherent panoramic registration are better matched to the low secondary ion currents available under static conditions. Furthermore, the "unlimited" m/z range in TOF MS allows the detection of high ions from polymers up to m/z 10000.

Bombardment of a solid with primary ions in the range of 5 – 25 keV leads to the erosion of consecutive surface layers. The majority of the evaporated material is released as neutral species and only small fraction is ionised. In principle, the same primary ion guns can be used in dynamic and static SIMS. The distinction between the two techniques is solely based on the number of primary ions impinging per unit of surface area.

Assuming that the sample can be considered as a lattice of atoms, the process of energy exchange between the penetrating primary ion and the sub-surface target material or lattice can be understood as a collisional cascade. Some of the initial momentum is directed back to the surface species and results in the removal of constituents from the outer surface layer. The process however is much more complicated because part of the energy is imparted also to the electrons, binding the atoms into molecules. The energy lost by a particle when it is brought to a standstill in the sample, amounts to 5 – 25 keV so that even a minor fraction is sufficient to break any chemical bond. It is estimated that the impact of a keV primary ion leads to "collisional" and "radiation" damage in a region of several nm in diameter around its trajectory. As a result, the molecular structure of the constituents within this volume does no longer correspond to that before impact. To retain the molecular information in S-SIMS, it is essential that no primary ion strikes again that region. Therefore, the total ion dose, i.e. the product of the primary ion flux or current density and the total analysis time, must be kept under a given so-called static limit.

The development of fast electronics and the resulting renaissance of TOF MS have provided inherent advantages for S-SIMS. The transmission is one to two orders of magnitude above that of quadrupoles and its inherent panoramic detection makes that secondary ions over the entire m/z range can be detected from a single primary ion pulse. The m/z range is only limited by the mass resolution, which can be boosted by using ultra-short primary ion bunches in the sub-nanosecond range. This also improves the mass accuracy significantly.

Chapter 3

Results and Discussion

3.1 Inter-calibration of nuclear microprobe laboratories

An inter-calibration was performed between all laboratories with nuclear microprobes.

For this purpose, dedicated reference samples were prepared by Partner 7/8 (Bordeaux) by sectioning cryofixed gelatin gel standard uniformly loaded with titanium at different concentrations. Thin freeze-dried sections were then analyzed using six different setups. PIXE was carried out to measure the Ti level whereas RBS and STIM allowed the normalization of results in terms of concentrations. After the analysis of 26 sections with a mean Ti concentration of 81 *micr*g/g dry weight, we observed a standard deviation of less than 16,4%. The standard deviation increased up to 20% for a mean Ti concentration of 600 µg/g (25 sections analyzed). This procedure was a pre-requisite before launching studies on animal and human skin samples previously exposed to TiO_2 nanoparticles. By this way, we proved the reliability and reproducibility of quantitative procedures usually employed in our community to derive absolute concentrations from nuclear microscopy.

3.2 Electron and Ion Microscopies on porcine and healthy human skin

The µ-PIXE elemental maps of skin cross-sections exhibit a clear delineation of the different strata without staining. The *stratum corneum* is rich in sulphur whereas the *stratum spinosum* is rich in phosphorous. The boundary with papillae between epidermis and dermis is clearly visible. The lateral resolution of about 1 µm was not sufficient to observe the *stratum granulosum* unambiguously, let alone the *stratum lucidum*. Occasionally, streaky images were obtained due to shrinkage of the samples. These images were discarded. In order to check the integrity of the samples, STIM-images were taken before and after the PIXE-measurement. If the STIM-images were not identical within accuracy limits, the PIXE-maps were discarded. Frequently, STIM- and Ti-PIXE-maps were overlayed to give morphological information as well as information on the Ti-distribution. When PIXE-images are compared to HRTEM-images a systematic

difference becomes apparent. Whereas in HRTEM-images individual corneocyte layers with a thickness of about 0.5 – 1 µm in the *stratum corneum disjunctum* are generally well separated by a few µm (see left image in figure 3.1), this is cannot easily observed in PIXE-maps. We see two possible reasons for this difference: first, the sample thickness is very different; any corrugation of a corneocyte layer or a cut which is not perpendicular to the corneocyte layer would lead to "overlapping" corneocyte layers in the ion microscopy maps (see right image in figure 3.1). Alternatively - or in addition - adjacent corneocyte layers which are held together by desmosomes could separate easily if by chance the ultra-thin cross-section does not contain desmosomes any more and penetrating liquids could separate the layers further. For thicker cross-sections this situation does not prevail. This difference has no consequences for the conclusions to be drawn but nicely illustrates that every microscopic technique "sees" what has been prepared, not necessarily the same before sample preparation. Apart from this difference results from HRTEM and PIXE agree very well.

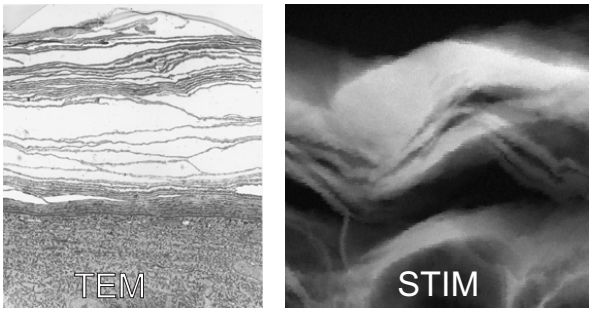

Fig. 3.1: Transmission electron microscopy image (TEM, left) and scanning transmission ion microscopy image (STIM, right) of the *stratum corneum* (upper half of the images). The skin cross sections have different thickness, < 1 µm for TEM and 14 µm for ion microscopy (in this case STIM). The thicker cross sections lead to overlapping corneocyte layers and therefore to a compacter appearance of the *stratum corneum* in the elemental maps.

The first surprise when looking with PIXE at skin cross-sections after exposure to formulations containing TiO_2 nanoparticles was that the Ti-map frequently showed that the formulation is distributed rather inhomogeneously on the *stratum corneum*. Large areas of the intact *stratum corneum* remain uncovered. An example is given in figure 3.2. What appears to be homogeneously distributed on a macroscopic scale (say a mm) is in fact inhomogeneous on a scale of several tens of µm. This inhomogeneous coverage is to some extent due to the topical application (skin furrows, hairs) and certainly also related to the spreading properties of the formulation on skin with different surface properties. This raises the question to what extent sun protection factors could be increased by a more homogeneous coverage. What is the smallest (laterally) possible inflammation (sunburn)?

In all HRTEM-images of both porcine and healthy human skin samples nanoparticles were found in the topmost 3 – 5 corneocyte layers in the *stratum corneum disjunctum* and never in the *stratum corneum compactum*. Many of the HRTEM-images did not include the *stratum spinosum*, but those which did exhibited no nanoparticles in the *stratum spinosum*. Typical examples are given in figure 3.3. This is in agreement with observations from PIXE-maps with a few exceptions. Despite great care

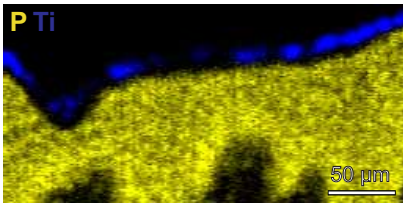

Fig. 3.2: Two element PIXE map (yellow: phosphorus, blue: titannium, 30×150 µm)of human skin. The phosphorus distribution matches the *stratum spinosum* which has a gap (corresponds to the *st. corneum compactum*) to the titanium layer. Titanium, i.e. TiO_2 nanoparticles are not homogeneously distributed over the skin surface.

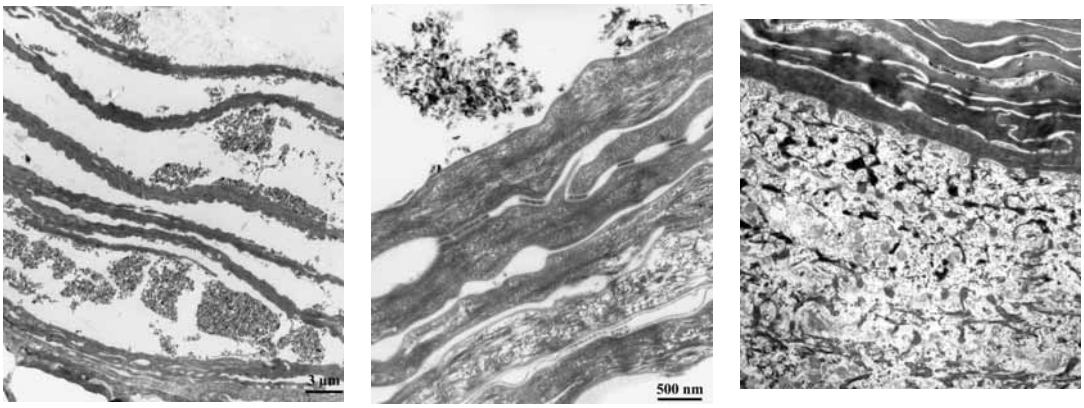

Fig. 3.3: HRTEM images of ultrathin cross sections of human skin showing the presence of TiO_2 particles in the topmost corneocyte layers only. The particulate matter in the *stratum corneum compactum* (right) was identified to be of organic origin.

with the sample preparation, it can happen that a small µm-sized portion of the *stratum corneum* with TiO_2 particles detaches and drops onto the cross-section suggesting deeper penetration. A clear example for preparation artefacts is one of the early sections, prepared with less experience, that shows clearly titanium deep in the *stratum spinosum* (figure 3.4).

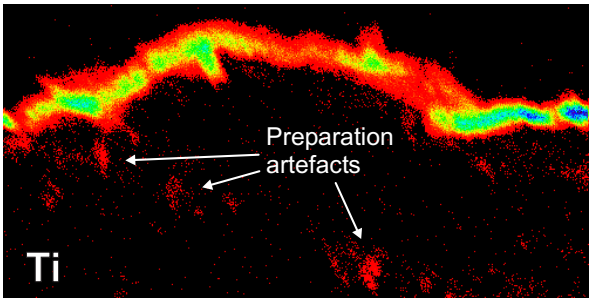

Fig. 3.4: PIXE map (400 µm × 190 µm) showing the titanium distribution The titanium spots deep in the *stratum spinosum* (below the superficial titanium layer) were proofed (using RBS) to be preparation artefacts due to less experienced handling.

A simple way to check whether this is a preparation artefact or not is possible by comparing elemental maps with the depth-sensitive backscattering signal from the relevant region in the map. When the titanium signal results from artefacts, the

titanium in a particular spot should be on one side of the skin cross section but not on the other. The RBS spectrum then shows either an edge like signal from "surface"-titanium at a characteristic backscattering energy (black spectrum in fig. 3.5) or a blurred titanium signal which results from a covered titanium source (red spectrum in fig. 3.5).

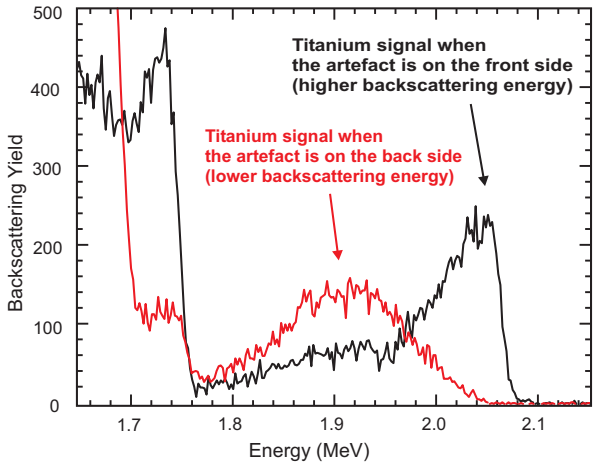

Fig. 3.5: Validating preparation artefacts by RBS-analysis. The two spectra are taken from a particular titanium spot in the *stratum spinosum* by measuring the front side (black), turning the sample and measuring the back side. The black spectrum shows the titanium uncovered, i.e. on the surface of the skin cross section; the red spectrum reveals the titanium covered by the skin cross section itself, thus proofing the titanium as a cross section surface contamination.

Another possibility is the use of secondary electrons and inspection of the front and back side of the sample. In most cases we could unambiguously identify preparation artefacts.

Another case is a sample taken from the margin between the human foreskin transplanted to SCID-mice and the murine skin. In this case, the *stratum corneum* was unusually thin and consisted of 3 corneocyte layers only (fig. 3.6 left). In this case, nanoparticles were observed in close contact with the *stratum lucidum* (fig. 3.6 right). The *st. lucidum* still is an effective barrier against nanoparticles.

Finally, we have an example for a microlesion, as indicated by the STIM-image, where deeper penetration close to the *stratum spinosum* was observed (see fig. 3.7 a) middle) contrary to the usual distribution of TiO_2 on top and in the topmost layers of the *stratum corneum* (see fig. 3.7 b) left). In an adjacent region, penetration until the *stratum spinosum* was observed without indication of a microlesion (see fig. 3.7 b) right), a feature which has been reported previously [Men04].

Common to all PIXE-maps is the fact that we never observed a coherent pathway for nanoparticle penetration nor a concentration profile suggesting a diffusive transport. We did not observe any effect of exposure time. Skin pre-treatment had an effect in a few cases: cleaning with ethanol (degreasing) enhances the penetration of the liposome formulation, a so-called fast transporter, but the nanoparticles were not transported beyond the *stratum corneum* (see fig. 3.8). This is in disagreement with tape stripping results [Ben00].

Partial stripping removed the *stratum corneum disjunctum* and the nanoparticles

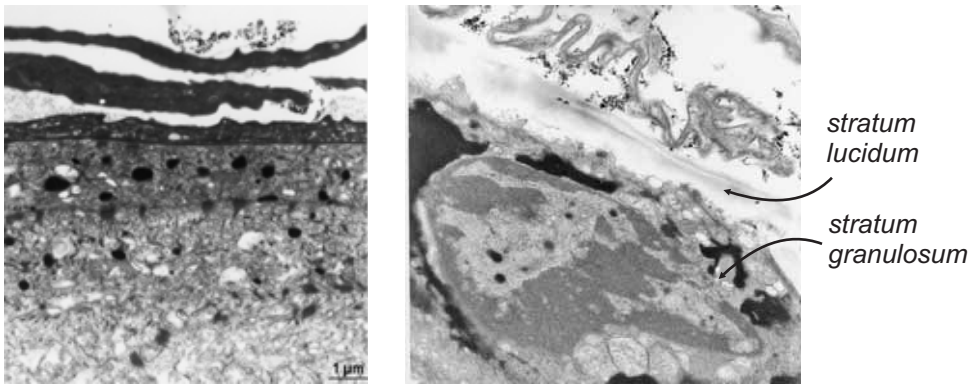

Fig. 3.6: Left: TEM micrograph of human foreskin skin transplanted to a SCID mouse. The *stratum corneum* is exceptionally thin. Right: In case of a thin *stratum corneum*, where only a few disjunct corneocyte layers are present, nanoparticles can come closer to the *stratum granulosum*; however, the intact *stratum lucidum* maintains the barrier function of the skin.

remained on the topmost corneocyte layer (see fig. 3.9). This HRTEM-image is one of the rare cases where the spreading was homogeneous. This fact indicates that the surface properties of the *stratum corneum* are probably responsible for the inhomogeneous coverage. In addition, the topical application might lead to instant desquamation of the topmost corneocyte layer leaving an uncovered region behind, a situation which does not pertain to the *stratum corneum compactum*. Alternatively, the spreading properties of Anthelios XL SPF60 might be favourable.

We have a few -PIXE images of sweat and sebaceous glands, none of them display uptake of nanoparticles. This might be fortuitous because of the small number of images.

The central conclusion of the observations discussed above is that nanoparticle penetration is not a diffusive process. Hence, no penetration kinetics could be studied. A typical nanoparticle with dimensions of 20 nm is not expected to diffuse fast enough, especially not in a viscuous medium. It appears that the nanoparticles are penetrated into the topmost corneocyte layers by mechanical action, i.e. passive transport. Recent studies of mechanically flexed skin report on greatly enhanced penetration compared to static skin. In one case, fluoresceinisothyocyanate (FITC) conjugated dextran beads of dimensions from 0.5 – 1 µm were used [Tin03]; the other study used fullerene-substituted phenylalanine (Baa) derivative of a nuclear localization peptide sequence (Baa-Lys(FITC)-NLS), termed a "nanoparticle" by the authors [Rou07]. It is not clear to what extent these results apply for TiO_2 nanoparticles as well. Future studies have to address this question in more detail. A consequence of these observations is that static Franz-cell studies are of limited use for nanoparticles. They might on the one hand overestimate the penetration due to truncated hair follicles, but on the other hand greatly underestimate the penetration into mechanically flexed skin.

We did not examine the clearance of the nanoparticles from the topmost layers of the *stratum corneum disjunctum*. However, it is logical that the desquamation with a typical rate of 0.5 µm per day is the important mechanism. It is not clear to what extent the application of soap and shower gels or exposure to seawater contribute to accelerated clearance. This would actually have consequences for the duration of the

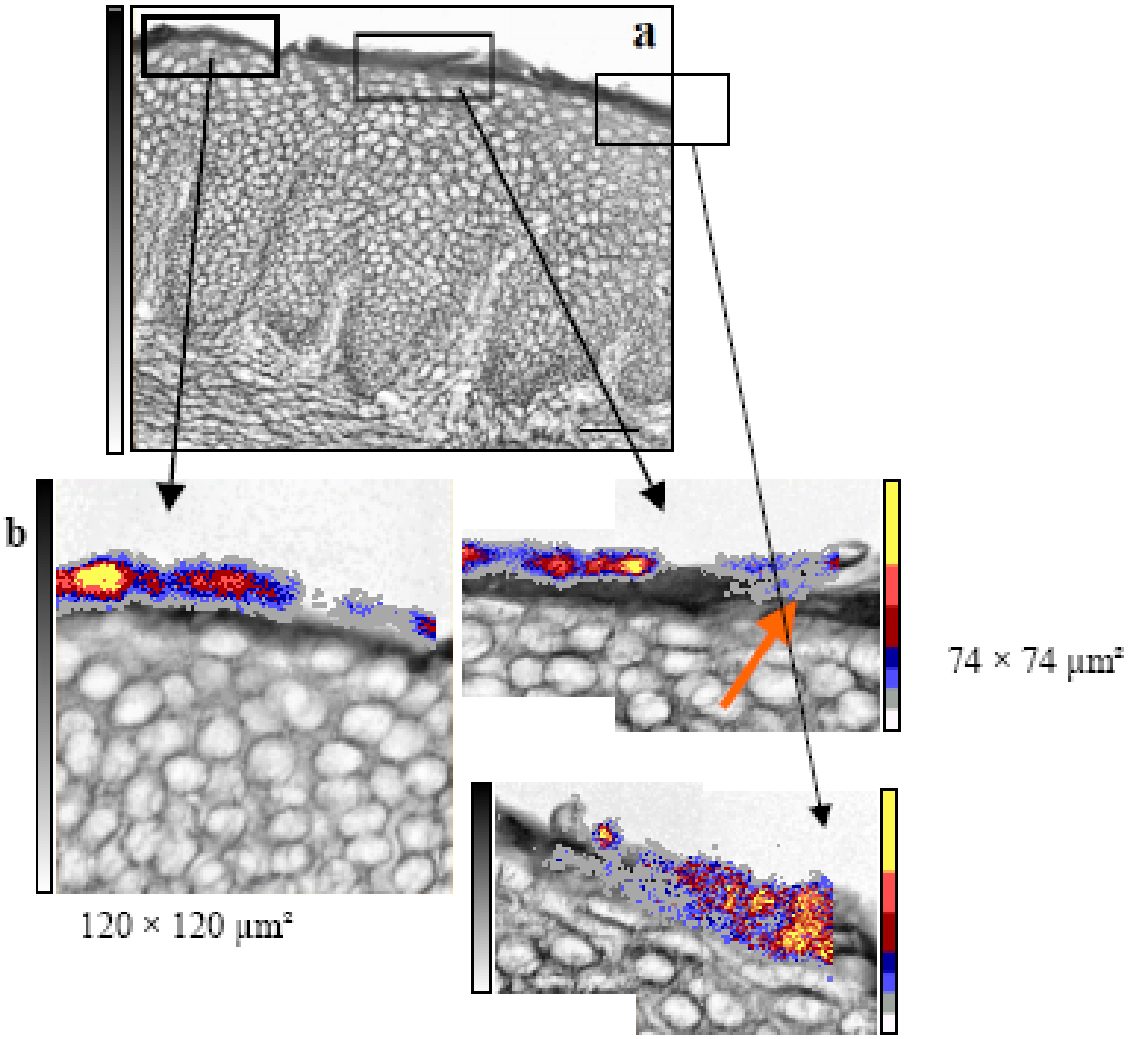

Fig. 3.7: a) large area STIM image and b) selected regions of interest with PIXE maps of titanium superimposed to the STIM images. Left: usual distribution of TiO_2 on top and in the topmost layers of the *stratum corneum*; middle: microlesion; right: penetration until the *stratum spinosum* without indication of a microlesion.

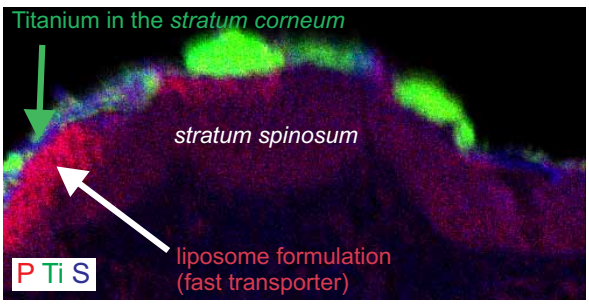

Fig. 3.8: Three element map of pig skin cross section with lipososome formulation, which is usually used as fast transporter. The enhanced phosphorus level in the *st. spinosum* indicates a good penetration of the liposome formulation. In contrast, the TiO_2 nanoparticles were not transported beyond the *st. corneum*.

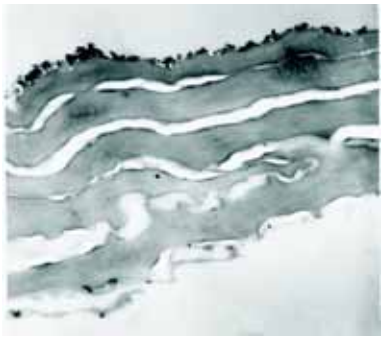

Fig. 3.9: TEM micrograph of human skin with stripped *stratum corneum disjunctum*. The TiO_2 nanoparticles are homogeneously spread over the topmost layer of the remaining *stratum corneum compactum*.

protecting action of the sunscreens.

3.3 Hair follicles studied by μ-PIXE

Apart from the intercellular pathway the follicular pathway was investigated. The number of images from sagittal cuts through hair follicles is limited. A good example of a μ-PIXE multicolour map for a cut which is almost sagittal is shown in figure 3.10. Apart from Ti found on top of the *stratum corneum* and at the entry of the follicle, Ti

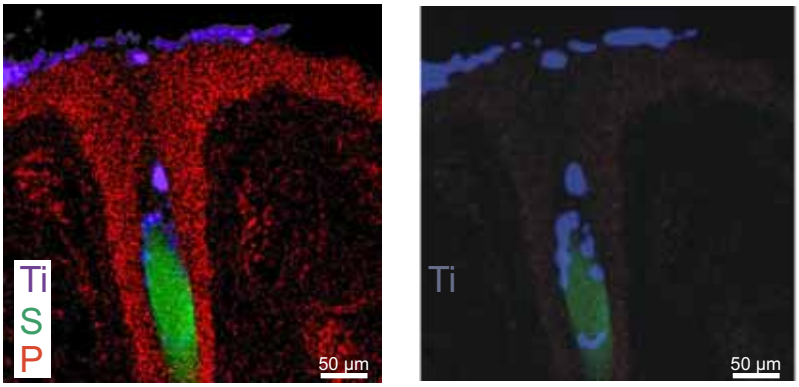

Fig. 3.10: Left: Three element map of a hair follicle which shows the titanium, i.e. the TiO_2 nanoparticles of the formulation rubbed into the follicle. Right: Same image as left, with enhanced Ti-signal and reduced S- and P-signal.

is observed around the sulphur-rich hair at a depth of almost 0.5 mm. Again there is no coherent pathway along the follicle. This suggests that the nanoparticles together with the formulation are introduced mechanically by stretching and compressing the follicle during application. We cannot corroborate the observation by Lademann ([Lad07]) that nanoparticles of a certain optimal dimension are transported by the surface structure of the hair, because our nanoparticles are much smaller than those of the optimal size and yet are penetrated deeply. We think it is the formulation which is actually pushed mechanically into the follicle and in this way the nanoparticles are pushed as well. No Ti is found in vital tissue. Unfortunately, we have no images of the bottom

of the hair follicle which could represent a weak barrier. In any case, the amount of material in hair follicles is small compared to the overall exposure. Clearance might proceed via secretion of sebum. It should be mentioned that occasionally we found hair follicles without Ti-signals, in agreement with [Lad99, Lad01].

3.4 Autoradiography and γ-ray counting on excised human skin

Radiolabeling was performed by the nuclear reaction ^{48}Ti(p,n)^{48}V ($T_{1/2}$ = 16 d) using chemically pure TiO_2 as powder target (rutile, about 20 nm diameter, R-HD2, Huntsman) at the Cyclotron at Kraków (partner 5). ^{48}V nuclei decay via positron emission (and electron capture) predominantly to the 2295.6 keV level of ^{48}Ti with a maximum energy for the positrons of 1720 keV. The prominent γ-rays at energies of 983.5 keV and 1312.1 keV are convenient for g-ray counting whereas the positron tracks are suitable for visualization in nuclear microemulsions. A pill of 100 mg pressed nanoparticles wrapped in 0.05 mm Al foil was irradiated with 17 MeV protons for 24 hours with a proton beam current of 1 μA. Two days after irradiation when most short-lived parasitic activities have decayed, the total activity of the target was 85 MBq. 1 Bq corresponded to 1.176 ng of TiO_2. The detection limit for our HPGe detector was lower that 0.03 ng of TiO_2. The irradiated TiO_2 was carefully mixed with hydrophibic basisgel (German Pharmaceutical Codex) with a concentration of 5 wt%. Large pieces of explanted human skin were delivered 2 – 3 hours after surgery of breast cancer. The samples were exposed to the radioactive formulation by softly rubbing it onto the outer part of the skin. After 2 hours exposure the formulation was carefully removed from the skin with ethanol and soap water until no activity was detectable in the wadding pads. After this cleaning procedure about 5 μg of TiO_2 per cm^2 remained in the skin samples. Several biopsies were cut from the samples and were fixed for 24 hours in formalin, then dried, immersed in paraffin and cut in a microtome perpendicular to the skin surface into 5 μm thick slices for autoradiography. For the HPGe measurements, slices were cut parallel to the outer surface of the skin in order to obtain at least some depth information. Figure 3.11 shows the amount of TiO_2 detected versus the slice number. The amount decreases rapidly from the *stratum corneum* towards the deeper parts. Due to the corrugation of the skin surface this represents an average over different depths and should not be misinterpreted as penetration into 30 – 50 μm. There is an elevated level in slice 6 which contained a sebaceous gland. However, the speculation that Ti entered the sebaceous gland was disproved by a subsequent autoradiography which exhibited a furrow.

In the nuclear microemulsions, individual positron tracks were visible. Thus it is easy to discriminate between dark spots of dust and dark spots surrounded by tracks due to radioactivity in figure 3.12.

Figure 3.13 shows a transverse cut through a hair follicle which exhibits radioactivity around the hair, but also further away. This image shows the strength and the weakness of the technique simultaneously. On the one side, it is ultrasensitive, on the other side we found no way of avoiding contaminations in a transverse cut. Our plan to

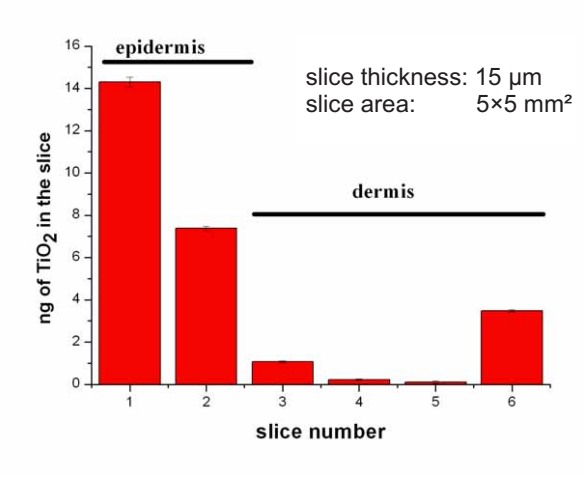

Fig. 3.11: Activation analysis of TiO_2 (HPGe measurements) applied to explanted skin. The skin slices were cut parallel to the sin surface. Slice number six contained a sebaceous gland.

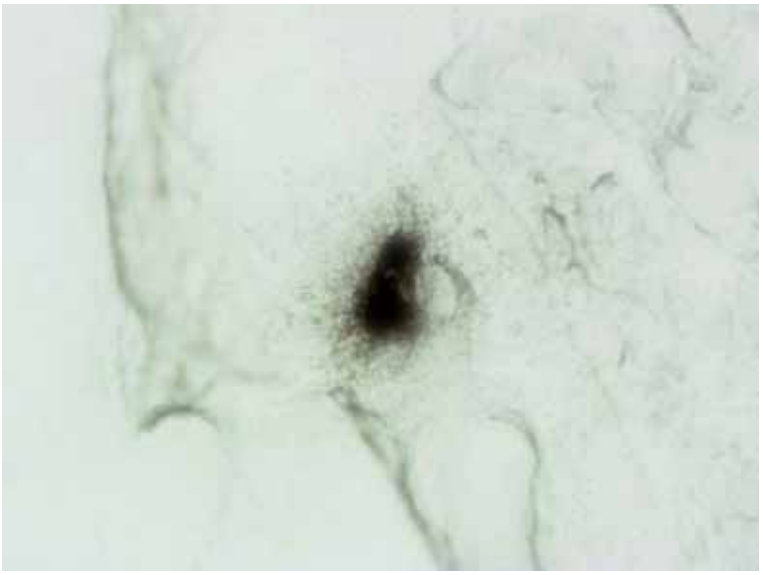

Fig. 3.12: Furrow showing individual positron tracks due to radiolabeled TiO_2.

soak the tissue with a sufficiently diluted microemulsion in greater depth, say several µm, to wait until all activity had decayed, and subsequently to remove the topmost contaminated slice did not work out. The microemulsion remained on the surface and did not penetrate deep enough. A second activation of a powder target yielded a much lower specific activity. For both reasons no further radiolabelling experiments were carried out.

3.5 Electron and Ion Microscopies on psoriatic skin

Psoriasis is a common skin disease where the barrier function is greatly impeded by hyperproliferation. The *stratum corneum* can be as thick as 100 µm, compared to the

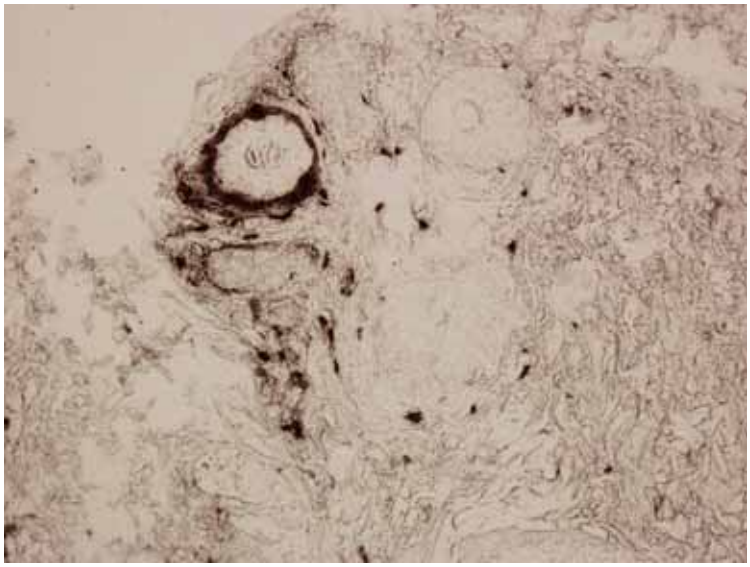

Fig. 3.13: Magnified image of an autoradiograph of a skin cross section (explanted human skin) which shows a follicle surrounded by activated TiO_2 (brown ring) after application of radiolabeled TiO_2 formulation.

normal 15 µm (see fig. 3.14). Moreover, there is no clear delineation between dead

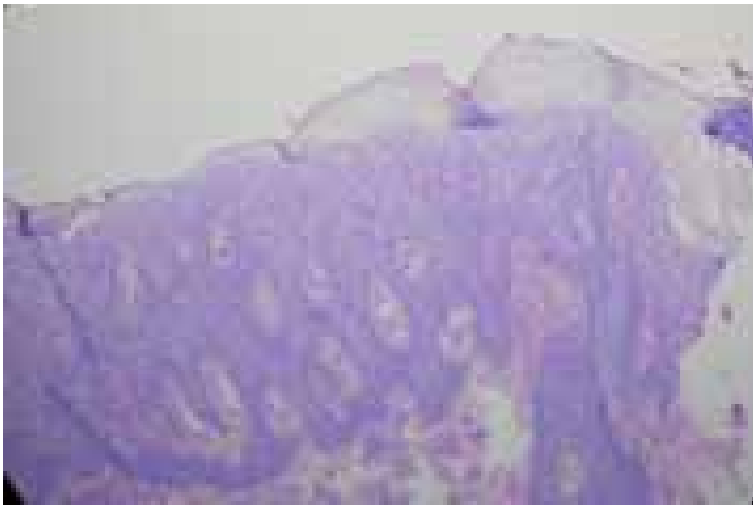

Fig. 3.14: Light microscopy image of a skin cross section with altered thickness of the *stratum corneum* (right part of the image) due to psoriasis.

corneocytes and vital keratinocytes. Four punch biopsies from patients with psoriasis were provided from partner 4 (Lisbon). A typical example of a multicolour µ-PIXE map is shown in figure 3.15. This image clearly shows that corneocytes and keratinocytes are intermingled such that one cannot speak of a barrier any more. The obtained Ti-maps were rather unsystematic. We found Ti on top of the *stratum corneum*, but occasionally also at much greater depth in contact with vital keratinocytes. These images resemble more a cross-section through a French croissant to which butter from the refrigerator is applied. Because the cross-section of psoriatic skin were rather brittle

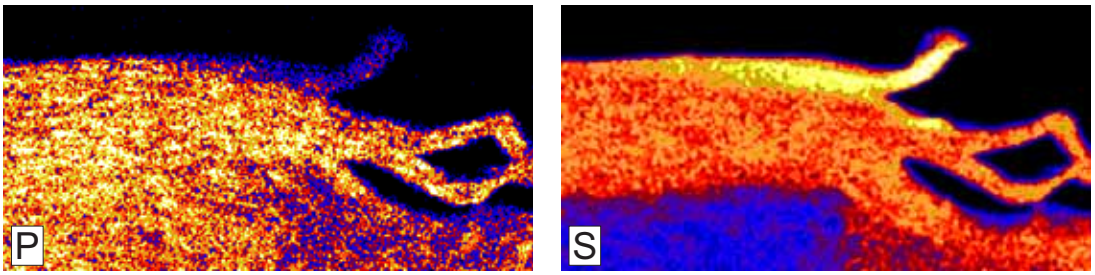

Fig. 3.15: PIXE maps (200 µm × 100 µm) of a cross section from psoriatic skin. The phosporus distribution (left) represents the distribution of vital cells. The sulfur distribution (right) represents the distribution of corneocytes. Both cell types, in healthy skin well separated, are intermingeld in the case of psoriasis.

preparation artefacts are almost unavoidable.

3.6 *In-vitro* studies

TiO_2 exists predominantly in the two polymorphs anatase and rutile with different absorption edges. Their cytotoxic effect under UV illumination is different [Say06]. We concentrated on ancoated anatase nanoparticles because their cytotoxic efficiency is much larger than that for rutile.

3.6.1 *In-vitro* effect of TiO_2-nanoparticles on various cell-lines

Titanium dioxide nanoparticles with 9 nm dimension (anatase, JA-1, uncoated) were dispersed in distilled water with 1:1000 dilution; doses of 15 µg/cm^2, 1.5 µg/cm^2, and 0.15 µg/cm^2 were applied to human immortalized keratinocytes (HaCaT), human immortalized sebocytes (SZ95), mouse immortalized fibroblasts (NIH 3T3), human dermal fibroblasts (HDF, primary culture), human primary melanocytes, and human monocyte-derived dendritic cells. The interaction of nanoparticles ion contact with cells was monitored up to four days. The morphology and eventual internalization was investigated by conventional microscopy. Apoptosis was studied using Annexin-V and Caspase-3. The cell permeability was studied via the $[Ca^{2+}]_i$ using fura 2. The cell proliferation was studied by an BrdU assay, by TUNEL, and in later studies by a combination of TUNEL and the proliferation specific nuclear marker Ki67. The cell viability was studied via MTT assay. We used differentiation and cell adhesion molecules (Western blot). The cellular response to contact with TiO_2 nanoparticles can be summarized as follows. Fibroblasts were the only cells where $[Ca^{2+}]_i$ was upregulated. A remarkable and fast internalization into the cytoplasm was observed for fibroblasts (see fig. 3.16), melanocytes, and dendritic cells. Internalization could proceed via endocytosis and non-phagocytic mechanisms [Gei05].

Apoptosis was not affected with the exception of fibroblasts and to a minor degree in dendritic cells (Annexin-V only). The proliferation was downregulated in keratinocytes, sebocytes and fibroblasts. We do not have data of melanocytes and dendritic cells. The number of viable cells was not affected with the exception of a decrease in fibroblasts

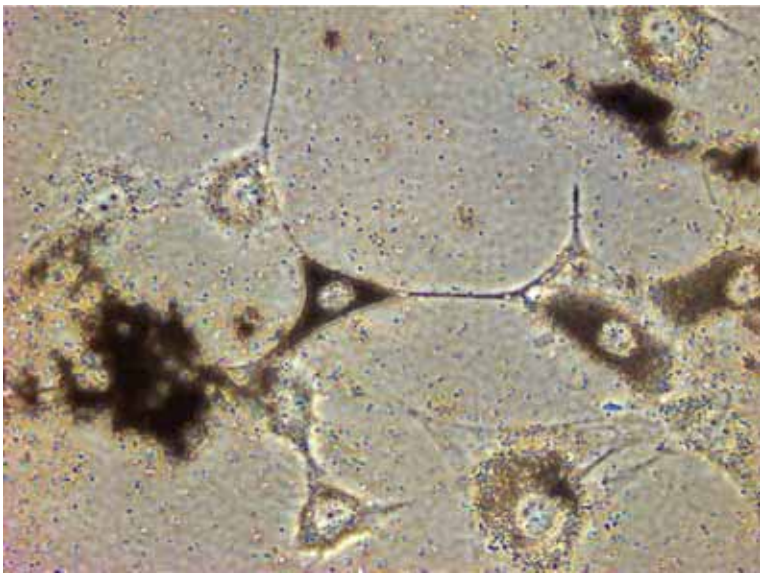

Fig. 3.16: A fast and remarkable internalization was observed for NIH 3T3 fibroblasts (exposure: 15 µg/cm^2 uncoated TiO_2 nanoparticles).

(see fig. 3.17) and to a minor extent in dendritic cells. For keratinocytes the expression of differentiation markers and adhesion molecules was downregulated (see fig. 3.18).

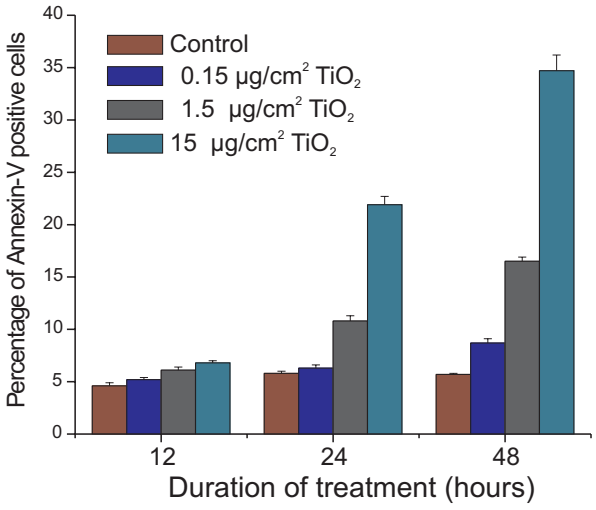

Fig. 3.17: With increasing TiO_2 dosis and exposure times the number of apoptotic NIH fibroblasts (Annexin-V positive) increases.

It should be stressed that significant changes in the various endpoints compared to the controls were observable - if they occurred - only after incubation of two to four days and in a dose dependent manner. Please note that all studies were performed by uncoated nanoparticles. Based on the microscopy studies presented above, it is rather unlikely that for topical applications of sunscreens containing coated nanoparticles on healthy skin doses as high as in the present *in-vitro* study will ever prevail, except for lesions.

Further studies were initiated with the human fibroblast cell line IMR90, the human

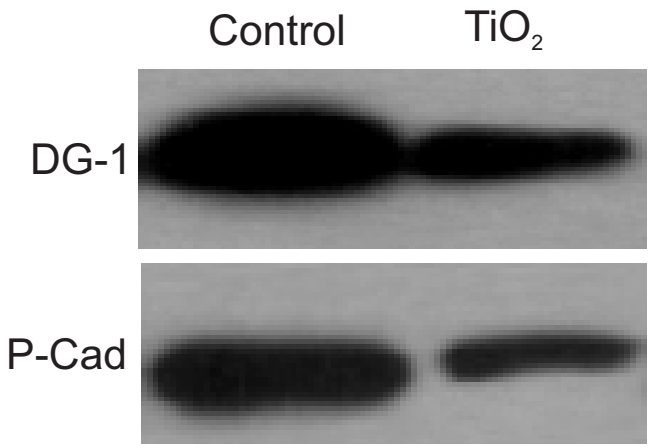

Fig. 3.18: The adhesion molecules desmoglein and P-cadherin of keratinocytes show a reduced expression in the presence of TiO_2.

keratinocyte cell line HaCat, the human primary keratinocyte cell (HPK, Invitrogen), and HeLa cells exposed to a suspension of uncoated TiO_2 particles (AMT-100, anatase, TAYCA) with an average diameter of 6 nm with different concentrations (10 and 100 µg/ml). Cell populations were grown to 60 – 80% confluency in 22 mm glass slides that have a plating area of 380 mm^2. The cell culture monolayers were treated with 2 ml of media supplemented with a suspension of 10 g/ml et 100 µg/ml TiO_2 for 24 – 48 – 72 h. These treatments result in exposure of the culture monolayers to 0.052 or 0.52 µg/cm^2 TiO_2. After incubation for 2 hours at 37C a fine precipitate appears on the cell culture monolayer. First results showed that there are cell line dependent morphological changes after TiO_2 exposure. Anomalies which look like cell membrane "retraction", membrane "holes", and membrane "ruffles" were observed (see fig. 3.19).

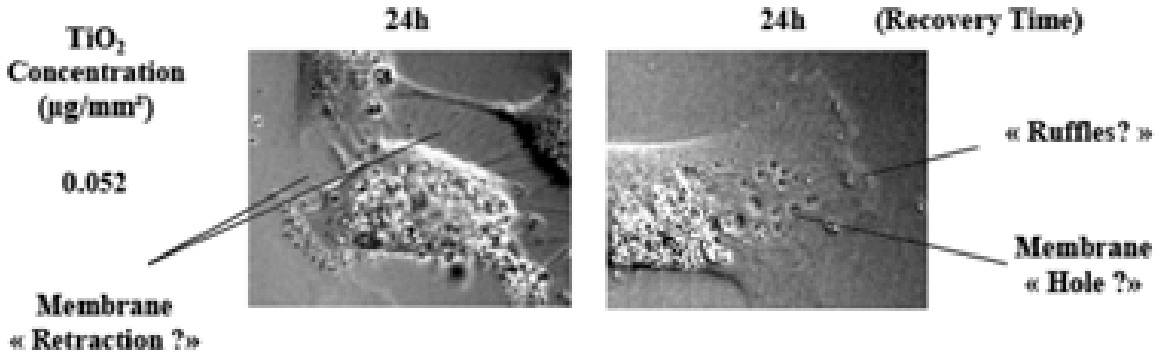

Fig. 3.19: Morphological changes after TiO_2 exposure, anomalies which look like cell membrane "retraction", membrane "holes", and membrane "ruffles" were observed.

3.6.2 *In-vitro* effect of TiO_2-nanoparticles on human epidermal psoriatic keratinocytes

We investigated the effect of TiO_2-exposure to human psoriatic epidermal keratinocytes.

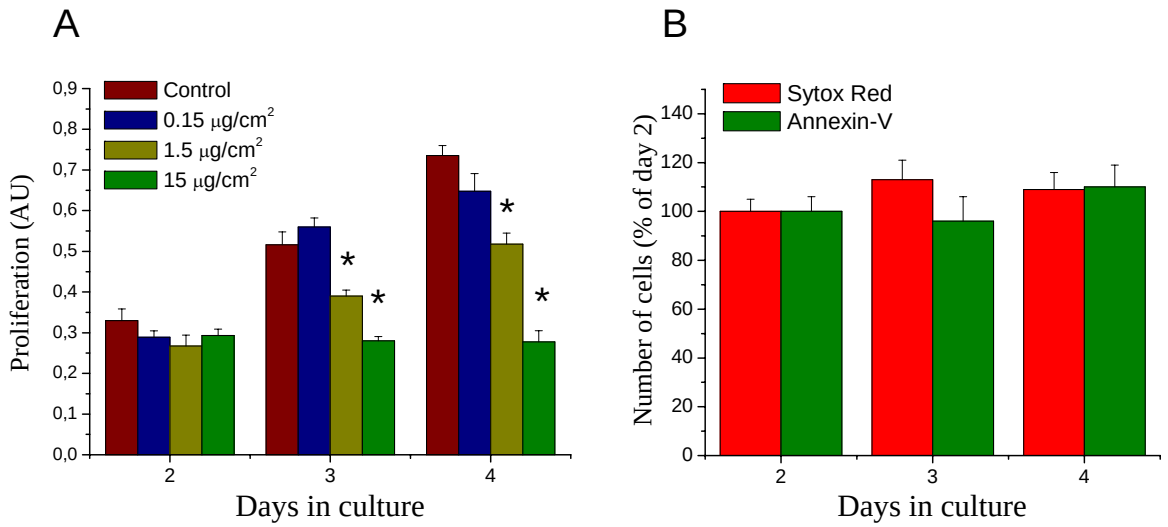

Fig. 3.20: Effect of *in-vitro* TiO_2-treatment on proliferation and cell viability of human psoriatic epidermal keratinocytes.

Figure 3.20 A) Cells were exposed by TiO_2-nanoparticles for up to 4 days then the number of viable cells was determined using MTT assays. Data represent mean ± SEM values of numerous determinations. Asterisks mark significant ($p<0.05$) differences compared to the daily-matched control. Figure 3.20 B) Cells were exposed by 15 mm/cm^2 TiO_2 for up to 4 days then the number of apoptotic (Annexin-V positive) and necrotic (Sytox Red positive) cells was determined. Data represent mean ± SEM values of numerous determinations. As was assessed by colorimetric MTT assays, TiO_2-nanoparticles (uncoated, 6 – 9 nm in diameter; anatase; used at 0.15 – 15 mg/cm^2 concentrations) suppressed the proliferation of psoriatic keratinocytes in time- and dose-dependent manners (Figure 3.20 A). However, TiO_2-exposure (again similar to those found on "healthy" epidermal keratinocytes) did not induce apoptosis (as measured by fluorimetric Annexin-V determination) or necrosis (as determined by fluorimetric Sytox Red accumulation in cell nuclei) (Figure 3.20 B). It appears, therefore, that the pathological status of epidermal keratinocytes did not alter their susceptibility to TiO_2-exposure.

In-vitro effect of TiO_2-nanoparticles on organ-cultured human scalp hair follicles Previous reports of NANODERM have implicated a potential importance of *in-vivo* transfollicular penetration of TiO_2-nanoparticles to the very vicinity of skin hair follicles. Therefore, we also intended to investigate the effect of direct TiO_2-exposure on various biological processes of organ-culture human scalp hair follicles obtained from waste materials of cosmetic or plastic surgery.

Human hair follicles were daily treated by TiO_2-nanoparticles (uncoated, 6 – 9 nm in diameter; anatase; used at 0.15 – 15 mg/cm^2 concentrations) and the elongation of

hair shaft was determined. As seen in figure 3.21A, up to day 5, neither concentration of TiO_2 affected the elongation. However, from day 7, the highest concentration of TiO_2 moderately yet significantly ($p<0.05$) suppressed hair growth.

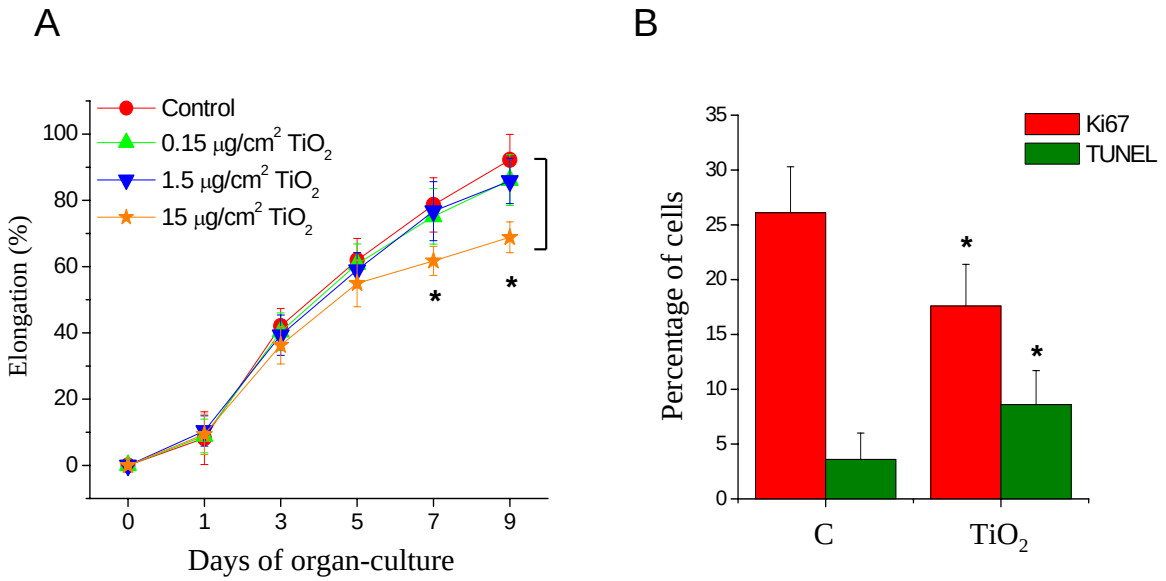

Fig. 3.21: Effect of *in-vitro* TiO_2-treatment on hair shaft elongation, proliferation and apoptosis of organ-cultured human hair follicles.

Figure 3.21 A) Human organ-cultured hair follicles (12 – 16 per group) were exposed by TiO_2-nanoparticles for up to 9 days then hair shaft elongation was determined. Data represent mean ± SEM values. Asterisks mark significant ($p<0.05$) differences compared to the daily-matched control. Figure 3.21 B) Statistical evaluation of Ki67 positive (proliferation marker) and TUNEL positive (apoptosis marker) cells in control (C) and 15 mg/cm^2 TiO_2-treated hair follicles at day 9 as a percentage of total cell number visualized by DAPI. Data represent mean ± SEM values. Asterisks mark significant ($p<0.05$) differences compared to control.

Using double Ki67/TUNEL immunofluorescence labeling on histological sections of the hair follicles, we have also found that this effect of 15 mg/cm^2 TiO_2 (at day 9) was also accompanied by the inhibition of the proliferation of the matrix keratinocytes of the hair follicle (Figure 3.21 B), similarly to data obtained on cultured epidermal keratinocytes (Figure 3.20). However, as opposed to findings on cultured epidermal keratinocytes, 15 mg/cm^2 TiO_2 treatment also elevated the number of TUNEL positive cells reflecting the induction of apoptosis (figure 3.21B).

In the frame of our pervious results that TiO_2-nanoparticles were internalized by cultured human epidermal melanocytes and that TiO_2-treatment inhibited their proliferation, we also tested whether TiO_2-exposure also affected melanogenesis in the hair follicles. We found that 15 mg/cm^2 TiO_2, again only at day 7 and 9, moderately yet significantly suppressed the melanin content of the follicles (see fig. 3.22).

Human organ-cultured hair follicles (12 – 16 per group) were exposed by TiO_2-nanoparticles for 9 days. Figure 3.22 A) Statistical evaluation of melanin content of the hair follicles as revealed by Fontana-Masson immunohistochemistry followed

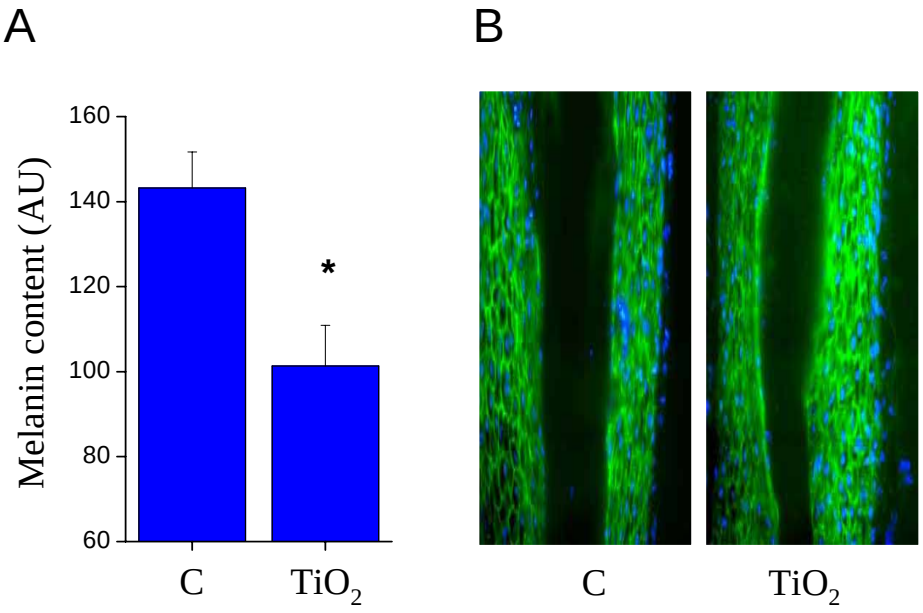

Fig. 3.22: Effect of *in-vitro* TiO_2-treatment on melanin content and the expression of the differentiation markers filaggrin in organ-cultured human hair follicles.

by image analysis. Data represent mean ± SEM values. Asterisks mark significant ($p<0.05$) differences compared to the control. Figure 3.22 B) Immunohistochemistry of the differentiation marker filaggrin in the distal outer root sheath keratinocyte layers of vehicle (Control) and 15 mg/cm^2 TiO_2-treated skin samples. Cell nuclei were visualized by DAPI.

Finally, we were also interested in whether TiO_2-exposure affects or not the differentiation process of the hair follicle. As revealed by immunofluorescence, 15 mg/cm^2 TiO_2 treatment, in contrast to our observation on cultured epidermal keratinocytes, did not significantly alter the expression of the differentiation marker filaggrin in the outer root sheath keratinocyte layers of the hair follicle (figure 3.22B).

In conclusion, our data suggest that prolonged direct exposure of high concentrations of TiO_2-nanoparticles may moderately modify such biological processes of organ-cultured human hair follicles as hair shaft elongation, proliferation, apoptosis, and melanogenesis.

3.6.3 *In-vitro* effect of TiO_2-nanoparticles on human epidermal psoriatic keratinocytes

Nanocrystalline titanium dioxide has been reported to generate reactive oxygen species (ROS) under UV illumination. Therefore, changes in the mechanical properties of human skin fibroblasts (American Type Culture Collection CCL-110), exposed to the oxidative stress induced by the presence of TiO_2 nanoparticles (average crystallite size of $\sim$ 6 nm, AMT-100 from Tayca© Corp.) and UV light, were studied using atomic force microscopy (AFM). The exposure of cells to the action of ROS was performed at low TiO_2 concentrations (4 mg/mL) and under illumination with low-intensity UVA

(8 mW/cm^2 and 20 mW/cm^2) or UVC (0.1 mW/cm^2). AFM measurements of the cell stiffness were carried out immediately after exposure of cells to the oxidative stress.

Exposure of human skin fibroblasts to UVA light at a power of 20 mW/cm^2 for up to 180 seconds had no effect on the cell stiffness. Similarly, exposure to TiO_2 nanoparticles alone at a dose of 4 µg/ml had no effects. Both exposures apparently are too low to induce measurable changes in cell elasticity. It should be noted that concentration of nano-TiO_2 we used was at least 20 times lower than the threshold employed in previous works. However, the combination of both exposures resulted in significant changes of the cellular Young's modulus which scaled with the UVA intensity. This is certainly due to the higher concentration of photo-generated ROS.

The addition of the antioxidant β-carotene suppressed the change in elasticity, demonstrating the high scavenging efficiency for the dominant ROS $O_2^{\bullet}$ - and $OH^{\bullet}$. Curcumin was much less efficient in this respect. A dramatic decrease in the cell stiffness was observed upon low-dose UVC irradiation, confirming the cytotoxicity of UVC exposure and indicating a high sensitivity of human fibroblasts to this part of the UV spectrum. The effect of UVC was so dominant that it was not possible to separate it from the effect of ROS on living cells after UVC illumination in the presence of TiO_2 nanoparticles. Therefore, it may be concluded that the early changes in cellular stiffness were more likely caused by the UVC radiation itself. The drop in cell stiffness already after 90 seconds of UV exposure suggests that damage occurs on the cell surface, e.g. in the cell membrane, transmembrane proteins or focal adhesion points that provide anchoring sites for the cytoskeleton. An increased level of ROS can also strongly influence the polymerization of actin fibers, thus leading to dramatic changes in the actin cytoskeleton reorganization and cellular elasticity.

3.7 *In-vivo* studies

Human foreskin grafts on SCID mice (protocol has been described in the previous reports) were treated under sterile conditions with a hydrophobic emulsion containing micronised TiO_2-nanoparticles (Anthelios XL F60, La Roche-Posay, France) in occlusion, for 1, 24 or 48 hours (to control mice, vehicle was applied). Animals were then euthanized and 6 mm-wide punch biopsies were taken from the human skin graft areas and processed for histology.

To assess the effect of micronized TiO_2-nanoparticles on the cellular viability (proliferation, apoptosis) of the skin cells, a series of immunohistochemical staining was performed. Using labelling of BrdU (proliferation marker), we found that TiO_2-treatment of human skin grafts did not modify the proliferation activities of epidermal keratinocytes (i.e., did not modify number of BrdU positive cells) (see fig. 3.23).

Grafts were exposed by TiO_2-nanoparticles for 48 hours then immunohistological determination of the proliferation marker BrdU was performed. Figure 3.23 A) BrdU positive epidermal keratinocytes (arrows). 3.23 B) Statistical evaluation of BrdU positive cells (per section) in control (C) and TiO_2-treated samples as a percentage of total cell number (mean ± SEM, 15 – 200 sections and 2 – 3 animals per group). Note the lack of effect of TiO_2-exposure.

In addition, by double labelling of Ki67 positive (hence proliferating) and TUNEL

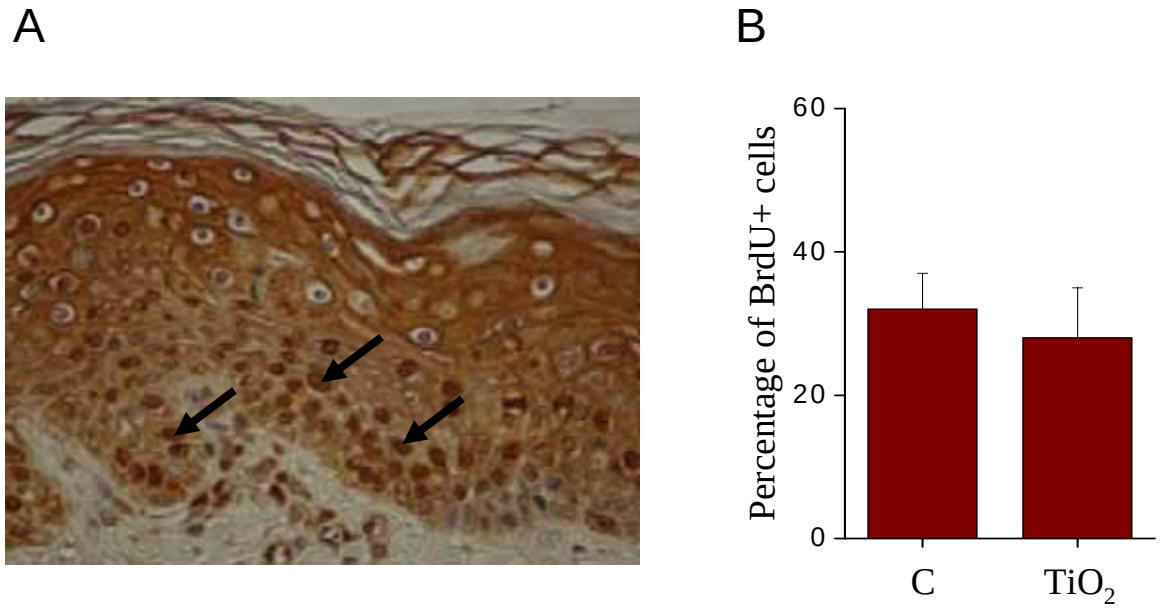

Fig. 3.23: Effect of *in-vivo* TiO_2-treatment on proliferation of human skin keratinocytes.

positive (hence apoptotic cells), we have also shown that the application of TiO_2-nanoparticles did not induce apoptosis in the skin cells (see fig. 3.24 A). Finally, using marker specific antibodies, we found that TiO_2-treatment did not significantly alter the expression of the basal epidermal keratinocyte-specific adhesion molecule P-cadherin (see fig. 3.24 B) or of the differentiation markers keratin-1, -10, and filaggrin (data not shown). These findings strongly argue for that TiO_2-exposure did not modify the viability, proliferation, apoptosis, differentiation, and adhesive properties of skin cells.

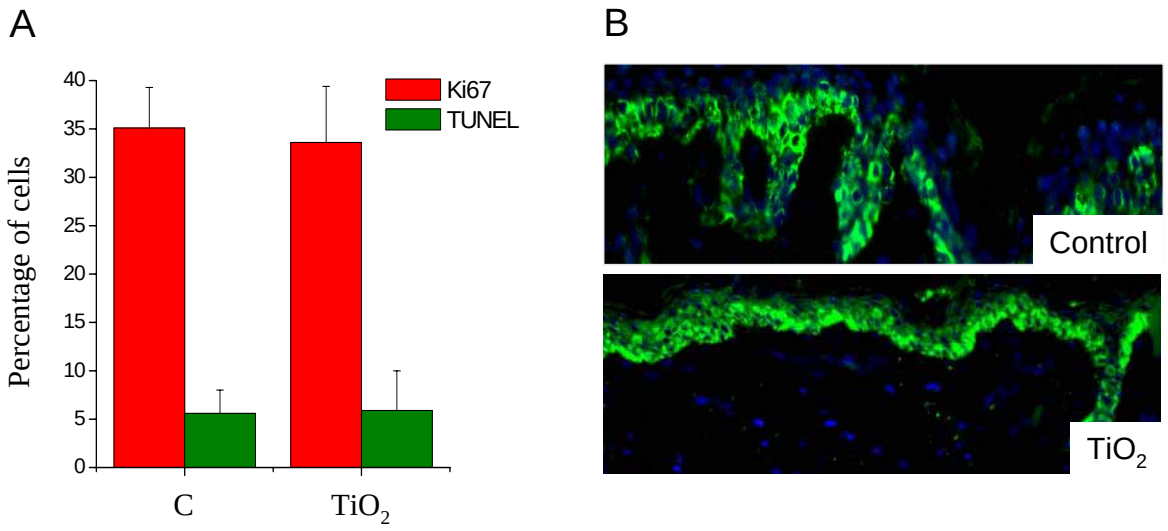

Fig. 3.24: Effect of *in-vivo* TiO_2-treatment on proliferation, apoptosis, and filaggrin expression of human skin keratinocytes.

Grafts were exposed by TiO_2-nanoparticles for 48 hours then immunofluorescence determinations were performed. Figure 3.24 A) Statistical evaluation of Ki67 positive

(proliferation marker) and TUNEL positive (apoptosis marker) cells in control (C) and TiO_2-treated samples as a percentage of total cell number (mean ± SEM, 15 – 200 sections and 2 – 3 animals per group). Figure 3.24 B) Immunohistochemistry of the adhesion molecule P-cadherin in vehicle (Control) and TiO_2-treated skin samples. During both procedures, cell nuclei were visualized by DAPI. Note the lack of effect of TiO_2-exposure.

3.8 Nanoparticle-formulation interaction

FT LMMS and S-SIMS were employed for the molecular characterisation, identification and possible quantification of the chemical interactions between the ingredients of a TiO_2-containing dermatological gel due to UV irradiation. Looking at the specificity in terms of information level, LMMS and S-SIMS inherently rank high because full molecular information (i.e. MW + structural fragments) is obtained. Both, S-SIMS and LMMS feature sufficient detection sensitivity to trace back the major components within one or few monolayers. The limits of the detection for both methods must be estimated to be in the range of 10000 – 100000 individual molecules. This brings the methods in the reach of nanoscale applications. The multilayer information depth in LMMS is an advantage in comparison to S-SIMS when accidental contaminants cover the surface of interest. Hydrophobic basisgel, isopropylmyristate gel, microemulsion-gel, polyacrylate gel were prepared with and without coated TiO_2-nanoparticles (Eusolex© T-2000). The different gels were analysed before and after UV-irradiation at a l of 365 nm at 100 W during 1 h. This corresponds to about 12 h of exposure in sunlight. Both FT LMMS and S-SIMS were used to verify the chemical composition in terms of original ingredients (to verify local heterogeneities on a mm scale), interaction products and changes due to the UV irradiation. The complementary application of both methods to all samples was needed to optimise the detection sensitivity of all components (ion yield of a given analyte is often high in LMMS and low in S-SIMS and vice versa) and to exploit the difference in information depth (monolayer in S-SIMS gives "cleaner" spectra but no information on subsurface components as opposed to FT LMMS). An overall reproducibility within 20 – 30% has been achieved. This is considered as an acceptable figure considering the experimental state of analytical techniques used, the innovative nature of the experiment and the complexity of the issue studied. From the huge amount of data obtained, it is found that the TiO_2 particles are especially present in the subsurface, not in the upper monolayer, for all 4 gels. On the other hand, the chemical composition of the upper monolayer gives intense signals from various contaminants, e.g. quaternary ammonium salts, silicones, UV-stabilisers used as additives in polymers, plasticisers. The detection of these contaminants reflect a preferential enrichment of such compounds in the outer surface layer. This is not at all surprising because e.g. the ammonium salts are soaps (tensio-active compounds) while also the other additives are especially useful when accumulated in the outer surface. However, for this study, the composition of the upper surface layer is in part driven by the surface-energy phenomena, and thereby for a significant part, by the contaminants (and not only by the ingredients!),. The application of UV irradiation, mimicking the exposure of the layer during 1 day to

natural sunlight, led to a modification of the surface and subsurface composition in only one of the 4 studied gel-systems. Specifically, the trometamol component in the polyacrylatgel, which moved to the subsurface after addition of Eusolex©, reappears again at the surface by UV irradiation. However, storing the sample for several days in the dark gives a similar behaviour. Otherwise stated, UV irradiation seems to accelerate the surface-energy driven reorganisation of the ingredients. Summing up, no evidence was found for the modification of the ingredients themselves or the formation of specific interaction products. In view of this negative result - positive for the consumer! - we refer the reader to the supplementary material provided on CD-ROM for further details.

Chapter 4

Conclusions

The NANODERM project is the broadest investigation of dermal penetration of TiO_2 nanoparticles thus far with a focus on the visualization of putative pathways. High resolution Transmission Electron Microscopy as well as various Ion Beam Analytical methods, above all -PIXE, were imployed. In addition, autoradiography using nuclear microemulsions and radiolabelled nanoparticles was performed.

Porcine skin, healthy human skin from biopsies and explants, human foreskin transplanted to SCID-mice, and psoriatic skin was examined with a variety of formulations containing TiO_2 nanoparticles as well as commercially available sunscreens. Various skin pre-treatments, exposure conditions and exposure times were applied

In all but a few cases Ti was detected on top of the *stratum corneum* and in the topmost layers of the *stratum corneum disjunctum* for healthy skin. Frequently the nanoparticles were aggregated. In most cases Ti-spots in vital tissue could be identified as preparation artefacts. In none of the roughly 500 images a coherent pathway of nanoparticles was observed, let alone a concentration profile characteristic of diffusive transport. Moreover, the type of formulation and the duration of exposure did not affect the penetration.

Hence, we conclude that the TiO_2 nanoparticles are penetrated into the topmost $3 - 5$ corneocyte layers by mechanical action and no diffusive transport takes place. Thus, penetration studies with static Franz-diffusion cells do not seem adequate for nanoparticles. Clearance is expected to proceed via desquamation. There is deep penetration into hair follicles, but not into vital tissue. Clearance is expected to proceed via sebum excretion.

No new species were detected by S-SIMS and LMMS due to the interaction of the formulations with coated TiO_2 nanoparticles without and with UV-light.

The interaction of cells with TiO_2 nanoparticles both coated and uncoated was studied both *in-vitro* and *in-vivo* by immuno-histochemical methods and AFM. The cellular response to TiO_2 nanoparticles was found to depend on the cell type; various endpoints were examined. The elasticity of cells was affected by uncoated TiO_2 nanoparticles and UV-light. The relevance of these observations on the cellular level is still an open question because the exposure is rather low, if it exists at all. Nevertheless, we conclude that for the sake of safety, direct contact of skin cells with TiO_2 nanoparticles should better be avoided, e.g. application of sunscreens into open wounds is not recommended.

The situation with psoriatic skin is less clear. Instead of a *stratum corneum* of about 10 – 15 µm thickness, psoriatic skin has a *stratum corneum* of about 100 µm thickness with corneocytes and vital keratinocytes intermingled. Here, there is no real barrier and TiO_2 nanoparticles can come into direct contact with vital cells. However, we have no evidence that the TiO_2 nanoparticles become systemic.

Summing up, we do not expect any health effects for the topical application of sunscreens containing TiO_2 nanoparticles (especially when coated) on healthy skin which are related to the particulate state.

The life cycle of TiO_2 nanoparticles was not examined in the present project and ecotoxicological aspects as well as possible subsequent absorption via other ports of entry, e.g. the gastro-intestinal tract [Jan94], should be considered in the future.

There are still a few open questions concerning e.g. sunburned skin with skin detachments - a typical misuse of sunscreens - or atopic skin. Furthermore, the role of microlesions is unclear. Maybe the largest uncertainty is related to the fact that two recent publications ([Rou07, Tin03]) demonstrated that mechanical flexion of skin can greatly enhance the penetration. A standardized apparatus for mechanical flexion should be developed.

Finally, each method has detection limits and long-term exposure might still lead to appreciable absorption. Thus the biokinetics, possible translocation and accumulation into secondary organs, and the excretion should be investigated.

Last but not least, although TiO_2 nanoparticles of much smaller dimensions than 20 nm, say 2 nm, are not in use in sunscreens, it is conceivable that they might nevertheless be present and adsorbed onto larger particles, a phenomenon well known in aerosol studies. Whether they can be isolated and whether they are more soluble in body fluids than their larger counterparts remains to be investigated.

PS: A huge amount of images and details presented in various meetings is made available as supplementary material on CD-ROM.

Chapter 5

Exploitation and Dissemination of Results

5.1 Publications

P. Aguer, L.C. Alves, Ph. Barberet, E. Gontier, S. Incerti, C. Michelet-Habchi, Zs. Kertész, Á.Z. Kiss, P. Moretto, J. Pallon, T. Pinheiro, J.-E. Surleve-Bazeille, Z. Szikszai, A. Verissimo, M.D. Ynsa. Skin morphology and layer identification using different STIM geometries. *Nucl. Instr. and Meth. in Phys. Res. B* **231**, 292 (2005).

E. Gontier, P. Barberet, Y. Barbotteau, K. Gáspár, C. Habchi, J. Hunyadi, S. Incerti, B. Kiss, A. Mavon, P. Moretto, T. Pouthier, M. Rosdy, M.D. Surlève-Bazeille, J.E. and. Ynsa. Micro-PIXE characterization of different skin models. *X-ray Spectrometry* **34**, 381 (2005).

Zs. Kertész, Z. Szikszai, E. Gontier, P. Moretto, J.-E. Surlève-Bazeille, B. Kiss, I. Juhász, J. Hunyadi, Á.Z. Kiss. Nuclear microprobe study of TiO_2-penetration in the epidermis of human skin xenograft. *Nucl. Instr. and Meth. in Phys. Res. B* **231**, 280 (2005).

Zs. Kertész, Z. Szikszai, I. Uzonyi, A. Simon, Á.Z. Kiss. Development of a bio-PIXE setup at the Debrecen scanning proton microprobe. *Nucl. Instr. and Meth. in Phys. Res. B* **231**, 106 (2005).

Zs. Kertész, Z. Szikszai, I. Uzonyi, A. Simon, Gy. Szabó, G.Á. Szíki, I. Rajta, Á.Z Kiss. The Debrecen micro beam analysis facility: Report of recent development and applications with special emphasize on bio-PIXE. *10th International Conference on Particle Induced X-Ray Emission and its Analytical Applications. Portoroz, Slovenia, 4-8 June, 2004. Proceedings* Seite 904 (2006).

B. Kiss, T. Bíró, I.B. Czifra, G. Tóth, Zs. Kertész, Z. Szikszai, Á.Z. Kiss, I. Juhász, J. Hunyadi. Investigation of TiO_2 penetration in human skin xenografts and its affect on cellular functions of human skin-derived cells. *Exp. Dermatol.* **submitted for publication**.

B. Kiss, Zs. Kertész, Z. Szikszai, E. Gontier, P. Moretto, J.-E. Surleve-Bazeille, Á.Z. Kiss, J. Hunyadi. Investigation of TiO_2-penetration in the epidermis of human skin xenografts. *Journal of the European Academy of Dermatology and Venereology* **18** (s2), 288 (2004).

J. Lekki, Z. Stachura, W. Dambros, J. Stachura, F. Menzel, T. Reinert, T. Butz, J. Pallon, E. Gontier, M.D. Ynsa, P. Moretto, Z. Kertesz, Z. Szikszai, A.Z. Kiss. On the follicular pathway of percutaneous uptake of nanoparticles: Ion microscopy and autoradiography studies. *Nucl. Instr. Meth. Phys. Res. B* **260**, 174–177 (2007).

A. Mavon, C. Miquel, O. Lejeune, B. Payre, P. Moretto. *In-vitro* percutaneous absorption and *in-vivo* stratum corneum distribution of an organic and a mineral sunscreen. *Skin. Pharmacol. Physiol.* **20**, 10–20 (2007).

A.D. Maynard, R.J. Aitken, T. Butz, V. Colvin, K. Donaldson, G. Oberdörster, M.A. Philbert, J. Ryan, A. Seaton, V. Stone, S.S. Tinkle, L. Tran, N.J. Walker, D.B. Warheit. Safe handling of nanotechnology. *Nature* **444** (7117), 267–269 (2006).

F. Menzel, T. Reinert, J. Vogt, T. Butz. Investigations of percutaneous uptake of ultrafine TiO_2 particles at the high energy ion nanoprobe LIPSION. *Nucl. Instr. Meth. Phys. Res. B* **219-220**, 82–86 (2004).

J. Pallon, A. Auzelyte, M. Elfman, M. Garmer, P. Kristiansson, K. Malmqvist, Ch. Nilsson, A. Shariff, M. Wegdén. An off-axis STIM procedure for precise mass determination and imaging. *Nucl. Instr. Meth. Phys. Res. B* **219-220**, 988–993 (2004).

J. Pallon, M. Garmer, A. Auzelyte, M. Elfman, K. Malmqvist, P. Kristiansson, Ch. Nilsson, A. Shariff, M. Wegdén. Optimization of PIXE-sensitivity for detection of Ti in thin human skin sections. *Nucl. Instr. Meth. Phys. Res. B* **231**, 274–279 (2005).

T. Pinheiro, J. Pallon, L.C. Alves, A. Veríssimo, P. Filipe, J.N. Silva, R. Silva. The influence of corneocyte structure on the interpretation of permeation profiles of nanoparticles across skin. *Nucl. Instr. Meth. Phys. Res. B* **in press** (2007).

A. Veríssimo, L.C. Alves, P. Filipe, J.N. Silva, R. Silva, M.D. Ynsa, E. Gontier, P. Moretto, J. Pallon, T. Pinheiro. Nuclear microscopy: A tool for imaging elemental distribution and percutaneous absorption *in-vivo*. *Microscopy Research and Technique* **70**, 302–309 (2007).

B. Vileno, M. Lekka, A. Sienkiewicz, S. Jeney, G. Stoessel, J. Lekki, L. Forró, Z. Stachura. Stiffness alterations of single cells induced by UV in the presence of nano-TiO_2. *Environmental & Science Technology* **accepted for publication** (2007).

5.2 Invited talks

17.9.2004 Arbeitsgemeinsachaft Oberflächenanalytik AOFA13 Dresden

21.9.2004 Matformum2004, Augsburg

25.-26.1.2005 Workshop "research need on nanoparticles", Brussels

26.8.2005 International Congress, *lavera* Naturkosmetik, Wennigsen

8.9.2005 EuroNanoForum2005 Edinburgh

7.-9.11.05 ECETOC, TiO_2 nanoparticles Barcelona

5.-7.4.2006 Nanotox workshop, Washington DC

28.4.2006 Bundesanstalt für Risikoforschung, Berlin

28.6.06 Psoriatic Skin, SCCP, Brussels

30.6.06 Industrieverband Körperpflege und Waschmittel, Frankfurt/M

4.-8.12.2006 International Symposium on Materials Chemistry, Mumbai

6.3.2007 CEFIC, Brussels

21.3.2007 OECD workshop on manufactured nanomaterials, Royal Society and Leopoldina, Dortmund

27.3.2007 Umweltforschungszentrum Leipzig-Halle, Leipzig

5.3 External expert services

Coordinator served as external export in committees (SCCP, SCENHIR) and contributed to dialogues and workshops (BfR, BAUA/BMU/UBA,OECD)

5.4 Interviews (selection)

Ökotest 4/2005

VDI Nanospotlight 4/2006 NANOKER

taz 11.07.2006

Bundesverband Naturkost und Naturwaren Einzelhandel e.V. 19.7.2006

Vital 3/2007

Schrot and Korn 2/2007

Deutschlandradio Kultur 15.5.2007, to be broadcasted

5.5 CDs of the 2nd Annual Report of NANODERM

Distribution of about 20 CDs on request

Chapter 6

Policy related Benefits

Within the NANODERM project various techniques were employed for the visualization of putative penetration pathways of TiO_2 nanoparticles through skin. No coherent pathways were detected, let alone concentration profiles characteristic for a diffusive mechanism. These studies greatly improve our knowledge of dermal penetration of nanoparticles compared to tape stripping and Franz diffusion cell studies, which yield very little depth information and integral results, respectively.

Based on electron and ion microscopies as well as autoradiography we do not expect any health effects for the application of sunscreens containing TiO_2 nanoparticles (especially when coated) on healthy skin which are related to the particulate state, because TiO_2 nanoparticles are mechanically penetrated into the topmost corneocyte layers of the *stratum corneum disjunctum* and do not enter into vital tissue. The exposure of TiO_2 nanoparticles to vital cells in healthy skin is below the detection limit of one nanoparticle in about 100 μm^3. Regarding the cellular response in contact with these nanoparticles and the very low exposure of vital cells, risk is supposed to be very low as well.

No particular additional regulations are required provided the cosmetic industries inform the costumer about nanoparticulate ingredients in their sunscreens and related products. This does not apply to applications for skin with impaired barrier function and misuse such as e.g. application of sunscreens to sunburned skin with skin detachments or open wounds.

Flexing the skin mechanically possibly enhances dermal penetration of TiO_2 nanoparticles and might substantially modify the above conclusion. A standardized device for skin flexion is badly needed to corroborate the two observations on flexed skin or to disprove this enhancement for TiO_2 nanoparticles.

The benefit of the NANODERM results for regulating and policy making bodies, both national and EU-wide, is that, on the one hand, sunscreens with TiO_2 nanoparticles as physical UV-filters to the best of our knowledge do not represent a health risk for healthy skin because of the lack of penetration into vital tissue; on the other hand, important data gaps, e.g. on skin with impaired barrier function and mechanically flexed skin as well as ecotoxicological effects after disposal to the environment and secondary unintentional incorporation have to be closed as soon as possible.

References

[Ben00] C. Bennat, C.C. Müller-Goymann. Skin penetration and stabilization of formulations containing microfine titanium dioxide as physical UV filter. *Int. J. of Cosmetic Science* **22**, 271–283 (2000).

[Bha97] P.J. Bhanu. Atomic Force Microscope: Providing new insights on the structure and function of living cells. *Cell Biology International* **21** (11), 683–684 (1997).

[Eng04] Royal Society Royal Academy of Engineering. Nanoscience and nanotechnologies, opportunities and uncertainties. Technischer Bericht (2004). Available at: http://www.nanotec.org.uk/finalReport.htm.

[Ful04] B. Fultz, J.M. Howe. *Transmission electron microscopy and diffractometry of materials*. Springer, Berlin, Heidelberg, 2. Ausgabe (2004).

[Gam06] A.O. Gamer, E. Leibold, B. van Ravenzwaay. The in vitro absorption of microfine zinc oxide and titanium dioxide through porcine skin. *Toxicology in Vitro* **20** (3), 301–307 (2006).

[Gei05] M. Geiser, B. Rothen-Rutlshauser, N. Kapp, S. Schuren, W. Kreyling, H. Schulz. Ultrafine particles cross cellular membranes by non-phagocytic mechanisms in lungs and in cultured cells. *Environ. Health Perspect.* **113**, 1555–1560 (2005).

[Gol98] Goldmann, Wolfgang H. and Galneder, Reinhard and Ludwig, Markus and Kromm, Alexander and Ezzell, Robert M. Differences in f9 and 5.51 cell elasticity determined by cell poking and atomic force microscopy. *FEBS Letters* **424** (3), 139–142 (1998).

[Gon04] E. Gontier, C. Habchi, T. Pouthier, P. Aguer, P. Barberet, Y. Barbotteau, S. Incerti, M.D. Ynsa, J.E. Surleve-Bazeille, Moretto P. Nuclear microscopy and electron microscopy studies of percutaneous penetration of nanoparticles in mammalian skin. *Journal of investigative Dermatology* **123** (2), 064 (2004).

[Jan94] P.U. Jani, D.E. McCarthy, A.T. Florence. Titanium dioxide (rutile) particle uptake from the rat GI tract and translocation to systemic organs after oral administrations. *Int. J. Pharm* **105**, 157–168 (1994).

[Jan95] P. Janmey. *Cell membranes and the cytoskeleton, In: Structure and dynamics of membranes.* Elsevier, Amsterdam (1995).

[Lad99] J. Lademann, H.J. Weigmann, C.H. Rickmeier, H. Barthelmes, H. Schaefer, G. Mueller, W. Sterry. Penetration of titanium dioxide microparticles in a sunscreen formulation into the horny layer and the follicular orifice. *Skin Pharmacol. Appl. Skin Physiol.* **2**, 247–256 (1999).

[Lad01] J. Lademann, N. Otberg, H. Richter, H.J. Weigmann, U. Lindemann, H. Schaefer, W. Sterry. Investigation of folllicular penetration of topically applied substances. *Skin Pharmacol. Appl. Skin Physiol* **14** (Suppl. 1), 17–22 (2001).

[Lad03] J. Lademann, H. Richter, N. Otberg, F. Lawrenz, U. Blume-Peytavi, W. Sterry. Application of a dermatological laser scanning confocal microscope for investigation in skin physiology. *J. Laser Phys.* **3**, 46–51 (2003).

[Lad07] J. Lademann, H. Richter, A. Teichmann, N. Otberg, U. Blume-Peytavi, J. Luengo, B. Weisz, U.F. Schaefer, C.M. Lehr, R. Wepf. Nanoparticles - An efficient carrier for drug delivery into the hair follicles. *European Journal of Pharmaceutics and Biopharmaceutics* **66** (2), 159–164 (2007).

[Lan97] A.B.G. Landsdown, A. Taylor. Zinc and titanium oxides: Promising UV-absorbers, but what influence do they have on the intact skin? *Int. J. Cosm. Sci.* **19**, 167–172 (1997).

[Lek99] M. Lekka, P. Laidler, D. Gil, J. Lekki, Z. Stachura, A. Z. Hrynkiewicz. Elasticity of normal and cancerous human bladder cells studied by scanning force microscopy. *European Biophysics Journal* **28** (4), 312 (1999).

[Lla98] Yvan Llabador, Philippe Moretto (*eds.*). *Nuclear microprobes in the life sciences.* World Scientific Publishing Co. Pte. Ltd. (1998).

[Mag04] B.M. Magnusson, Y.G. Anissimov, S.E. Cross, M.S. Roberts. Molecular size as the main determinant of solute maximum flux across the skin. *J. Invest. Dermatol* **122** (4), 993–999 (2004).

[Mav07] A. Mavon, C. Miquel, O. Lejeune, B. Payre, P. Moretto. In vitro percutaneous absorption and in vivo stratum corneum distribution of an organic and a mineral sunscreen. *Skin. Pharmacol. Physiol.* **20**, 10–20 (2007).

[Men04] F. Menzel, T. Reinert, J. Vogt, T. Butz. Investigations of percutaneous uptake of ultrafine TiO_2 particles at the high energy ion nanoprobe LIPSION. *Nucl. Instr. Meth. Phys. Res. B* **219-220**, 82–86 (2004).

[Noh07] Gerhard J. Nohynek, Jürgen Lademann, Christele Ribaud, Michael S. Roberts. Grey Goo on the Skin? Nanotechnology, Cosmetic and Sunscreen Safety. *Critical reviews in toxicology* **37** (3), 251–277 (2007).

[Pfl01] F. Pflücker, V. Wendel, H. Hohenberg, E. Gärtner, T. Witt, S. Pfeiffer, R. Wepf, H. Gers-Berlag. The human stratum corneum layer: An effective barrier against dermal uptake of different forms of topically applied micronised titanium dioxide. *Skin Pharm. Appl. Skin Physiol.* **14 Suppl.** (92-97) (2001).

[Rou07] J.G. Rouse, J. Young, J.P. Ryman-Rasmussen, A.R. Barron, N.A. Monteiro-Riviere. Effects of mechanical flexion on the penetration of fulleren amino acid-derivatized peptide nanoparticles through skin. *Nanoletters* **7** (1), 155–160 (2007).

[Say06] Christie M. Sayes, Rajeev Wahi, Preetha A. Kurian, Yunping Liu, Jennifer L. West, Kevin D. Ausman, David B. Warheit, Vicki L. Colvin. Correlating Nanoscale Titania Structure with Toxicity: A Cytotoxicity and Inflammatory Response Study with Human Dermal Fibroblasts and Human Lung Epithelial Cells. *Toxicol. Sci.* **92** (1), 174–185 (2006).

[Sch02] J. Schulz, F. Hohenberg, F. Pflücker, B. Gärtner, T. Will, S. Pfeiffer, R. Wepf, V. Wendel, H. Gers-Berlag, K.P. Wittern. Distribution of sunscreens on skin. *Adv. Drug Deliv. Rev.* **54 Suppl. 1**, 157–163 (2002).

[Str06] F. Stracke, B. Weiss, C.M. Lehr, K. König, U.F. Schaefer, M. Schneider. Multiphoton microscopy for the investigation of dermal penetration of nanoparticle-borne drugs. *J. Invest. Dermatol.* **126** (10), 2224–2233 (2006).

[Tan96] M.H. Tan, C.A. Commens, L. Burnett, P. Snitch. A pilot study on the percutaneous absorption of microfine titanium dioxide from sunscreens. *Austr. J. Dermatol.* **37**, 185–187 (1996).

[Tin03] S. S. Tinkle, J. M. Antonini, B. A. Rich, [JR] Roberts, R. Salmen, K. DePree. Skin as a route of exposure and sensitization in chronic beryllium disease. *Environ Health Perspect* **111**, 1202–1208 (2003).

[Wei99] H.J. Weigmann, J. Lademann, H. Meffert, H. Schaefer, W. Sterry. Determination of the horny layer profile by tape stripping in combination with optical spectroscopy in the visible range as a prerequisite to quantify percutaneous absorption. *Skin Pharmacol. Appl. Skin Physiol* **12**, 34–45 (1999).